Author final version

Investigating the Mapping of Chromophore Excitations onto the Electron Detachment Spectrum: Photodissociation Spectroscopy of Iodide Ion-Thiouracil Clusters

Kelechi O. Uleanya and Caroline E. H Dessent*

Department of Chemistry, University of York, Heslington, York YO10 5DD, U K.

* Corresponding author: caroline.dessent@york.ac.uk

KOU Orchid: https://orcid.org/0000-0003-2017-1360

CEHD Orchid: https://orcid.org/0000-0003-4944-0413

Abstract

Laser photodissociation spectroscopy (3.1-5.7 eV) has been applied to iodide complexes of the non-native nucleobases, 2-thiouracil (2-TU), 4-thiouracil (4-TU) and 2,4-Thiouracil (2,4-TU) to probe the excited states and intracluster electron transfer as a function of sulphur atom substitution. Photodepletion is strong for all clusters (I^-·2-TU, I^-·4-TU and I^-·2,4-TU) and is dominated by electron detachment processes. For I^-·4-TU and I^-·2,4-TU, photodecay is accompanied by formation of the respective molecular anions, $4\text{-}TU^-$ and $2,4\text{-}TU^-$, behaviour that is not found for other nucleobases. Notably, the I^-·2TU complex does not fragment with formation of its molecular anion. We attribute the novel formation of $4\text{-}TU^-$ and $2,4\text{-}TU^-$ to the fact that these valence anions are significantly more stable than $2\text{-}TU^-$. We observe further similar behaviour for I^-·4-TU and I^-·2,4-TU relating to the general profile of their photodepletion spectra, since both strongly resemble the intrinsic absorption spectra of the respective uncomplexed thiouracil molecule. This indicates that the nucleobase chromophore excitations are determining the clusters' spectral profile. In contrast, the I^-·2-TU photodepletion spectrum is dominated by the electron detachment profile, with the near-threshold dipole-bound excited state being the only distinct spectral feature. We discuss these observations in the context of differences in the dipole moments of the thionucleobases, and their impact on the coupling of nucleobase-centred transitions onto the electron detachment spectrum.

1 Introduction

The production of low-energy secondary electrons when high-energy radiation passes through biological molecules is a well-known phenomenon.[1,2] In biological systems, these low-energy electrons (≤10eV) can induce single and double-strand breaks in DNA, leading to mutations and genetic damage.[3-7] Quantum chemistry calculations have revealed that the nucleobase may be the initial site of electron attachment in DNA, with the resulting transient negative ion (TNI) corresponding to either a valence-bound anion via attachment to the base's π orbital or a dipole-bound anion.[8-11] Experiments probing dissociative electron attachment have shown that an initially formed dipole-bound state can act as a gateway to the valence-bound anion.[12] Due to the importance of low-energy electron-nucleobase interactions, a wide range of experiments have been performed to characterise the molecular dynamics involved.[13-20] One such series of experiments have involved iodide ion-nucleobase clusters.[21-29] Photoexcitation of such clusters can be accomplished in the gas-phase, providing a highly-controllable environment for probing low-energy electron-nucleobase coupling. The experimental approach is based on the concept that the iodide ion is photodetached to produce a 'spectator' iodine atom and a low-energy free electron with a well-defined kinetic energy that can be captured by the adjacent molecule.[27,30] The resulting TNI dynamics can then be monitored either *via* time-resolved photoelectron spectroscopy or photofragment action spectroscopy.

In this work, we present the first study of complexes of iodide with the non-native nucleobases, 2-thiouracil (2-TU), 4-thiouracil (4-TU) and 2,4-thiouracil (2,4-TU) which are illustrated in Scheme 1. We aim to probe how the cluster excited states are modified by the presence of one or more sulphur atoms in a non-native nucleobase. Thiolated nucleobases are synthetic analogues of native nucleobases that have been applied in radiation therapy and photodynamic therapies for some time,[31-34] motivating theory and experiments to understand their fundamental photochemical and photophysical behavior. Investigations have focused on understanding their photodynamics through comparison to native nucleobase excited-state potential energy surfaces and relaxation pathways.[35-48] Given that thionucleobases are employed in both radiation therapy and phototherapy, we aim here to obtain novel experimental information on how free electrons interact with thiolated nucleobases, both in the electronic ground and excited states. [49-52]

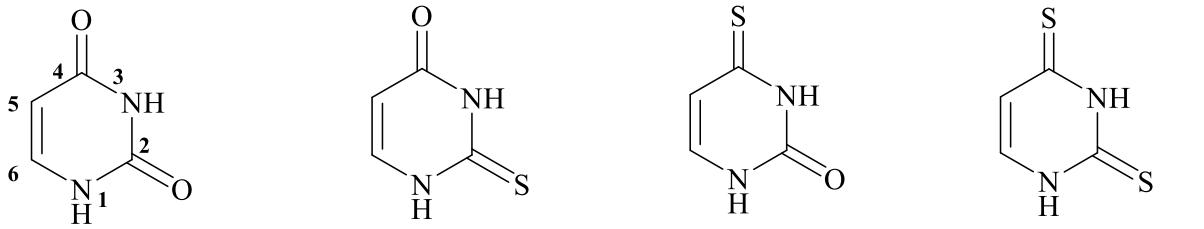

Scheme1 Schematic diagram of uracil (U), 2-thiouracil (2-TU), 4-thiouracil (4-TU) and 2,4-Thioracil (2,4-TU), illustrating how the C_2 - C_4 oxygens of uracil are replaced with sulphur.

Low-energy interactions with 2-thiouracil have been studied recently in a crossed-beam apparatus by Abdoul-Carime and co-workers.[49,51] Electron-attachment was shown to produce three major anionic fragments, with deprotonated 2-thiouracil being the major product, followed by the thiocyanate anion and the sulphur anion. The loss of hydrogen to form the deprotonated anion was initially suggested to occur from a mixture of carbon or nitrogen sites,[49,50] but was later found to arise from rupture of the N-H bond.[51] It was also established that molecular dissociation resulted from the initial step of dissociative electron attachment occurring through dipole-bound anion formation. Further experiments with 1-methyl-2-thiouracil gave fragments in line with this pattern of dissociative electron attachment, where significant loss of the methyl group from the N1 position was also seen.[51] No work has been conducted to date to characterise the low energy electron scattering properties of 4-TU and 2,4-TU. We note that the electronic spectrum of the deprotonated form of 2-TU has been studied recently via laser photodissociation,[53] and photodetachment photoelectron spectroscopy has been employed to characterize the molecular anions, $[4\text{-TU}]^-$ and $[2,4\text{-TU}]^-$.[54,55]

2 Experimental Method

UV photodissociation experiments were conducted using a modified AmaZon (Bruker) ion-trap mass spectrometer that has been converted for laser-interfaced mass spectrometry (LIMS) as described previously.[56,57] The $I^- \cdot$2-TU, $I^- \cdot$4-TU and $I^- \cdot$2,4-TU clusters were generated by electrospraying solutions of thionucleobases and iodide in 98% acetonitrile and 2% deionized water (solutions of 1×10^{-4} mol dm^{-3}, mixed with a CsI solution at 1×10^{-4} mol dm^{-3}). 2-TU was purchased from Acros organics, 4-TU and 2,4-TU from Sigma, and CsI from Avocado

Research Chemicals Limited. All chemicals were used without further purification.

UV photons produced by an Nd:YAG (10 Hz, Surelite) pumped optical parametric oscillator (OPO) (Horizon) laser were used to irradiate mass isolated clusters across the range 400–218 nm (3.1–5.7 eV). Scans were conducted with a 2 nm step size and ion depletion of the mass-selected clusters were taken as equivalent to gaseous absorption using the following:

$$\text{Photodepletion intensity} = \frac{In\left(\frac{IntOFF}{IntON}\right)}{P\lambda} \quad (1)$$

where P is the tuneable laser power (mJ), and λ is the wavelength (nm). Photodepletion intensities were averaged at each wavelength and plotted against photon energy. Photofragment action spectra were also acquired, with spectra being produced using:

$$\text{Photofragmentation production} = \frac{\left(\frac{IntFRAG}{IntOFF}\right)}{P\lambda} \quad (2)$$

An Orbitrap Fusion Tribrid mass spectrometer (Thermo Fisher Scientific, Waltham, MA, USA) with an ESI source was employed to perform higher-energy collision dissociation (HCD) to explore the ground-state fragmentation characteristics of the clusters. HCD fragmentation using the Orbitrap mass spectrometer gives tandem mass spectrometry which is similar to triple quadrupole fragmentation.[58-60] The instrument was operated with the following parameters: sweep gas flow rate, 0.; sheath gas flow rate, 2.0; aux gas flow rate, 2.5; ion transfer tube temperature, 275 ^{o}C; vaporizer temperature, 30 $^{\circ}$C; MS1 detector, Ion Trap; MS1 scan range, 80–300; MS1 maximum injection time 100 μs; MS2 detector, Ion trap; MS2 maximum injection time, 100 ms. HCD collisional energy was varied between 0% and 40%.

Electronic structure calculations were conducted using Gaussian 09.[61] Cluster structures investigated were based on the six tautomers of the thiouracils. These were optimized at the B3LYP/6-311++G(2d,2p) level, with 6-311G(d,p)/SDD for I. The vertical dipole moment (i.e. the dipole moment of the neutral cluster at the ground-state geometry of the anionic cluster) of the clusters was calculated at the MP2/6-311++G(2d,2p) level, with 6-311G(d,p)/SDD for I. Global energy minima were confirmed for all optimized structures by performing frequency calculations. Time-dependent density functional theory (TDDFT) calculations were performed on the lowest-energy optimised tautomers of the I^{-}·2-TU, I^{-}·4-TU and I^{-}·2,4-TU clusters to assign the excited-state transitions. Several functionals were tested, with the calculations

presented representing the best match to experiment.

3 Results

3.1 Geometric structures

Fig. 1 shows the lowest-energy structures of the I^-·2-TU, I^-·4-TU and I^-·2,4-TU clusters. (I^-·TU will be used when we are discussing the group of clusters.) The calculated structures are in good agreement with previous calculations of similar systems.[26,28,29] Additional calculations were conducted on other tautomers (Section S1, ESI), but the resulting cluster structures were found to have higher relative energies. In the lowest-energy structures (Fig. 1), the iodide ion hydrogen bonds to the nucleobases in a planar geometry through the N1 H and the C6 H. At this location, the iodide ion is bound close to the axis of the permanent dipole moment of the thiouracil (Section S2, ESI).

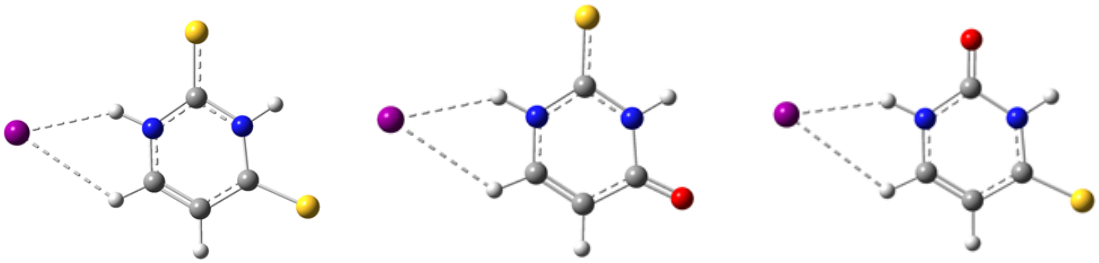

a b c

Fig. 1 Global minima geometric structures of a) I^-·2,4-TU, b) I^-·2-TU and c) I^-·4-TU clusters obtained at the B3LYP/6-311++G(2d,2p) level of theory with SDD on I.

Table 1 displays the calculated vertical detachment energies (VDEs), binding energies and the vertical dipole moments for the clusters. We note that the calculated vertical dipole moments indicates that all three clusters are sufficiently polar to support a dipole-bound state.[62-64] The VDEs of the three clusters are similar to that of the native nucleobase cluster, I^-·U. As the experimentally measured VDE of I^-·U is 4.11eV, while the calculated VDE is 4.30 eV,[26] we expect that the experimental values for the I^-·TU clusters are also likely to be around 4.1 eV. I^-·4-TU and I^-·2,4-TU are calculated to possess very similar vertical dipole moments and cluster binding energies, a result that is unsurprising given that 4-TU and 2,4-TU have similar dipole moments.[65] In contrast, the dipole moment of 2-TU is much closer to that of uracil. Indeed, the dipole moment of uracil derivatives is known to increase significantly on thialation

at the C4 position.[65]

Table 1. Calculated vertical detachment energies (VDE), cluster binding energies (BE),[a] and vertical dipole moments,[b] using B3LYP with the 6-311++G (2d,2p)/SDD basis set.

Cluster	**I^-·2,4-TU**	**I^-·2-TU**	**I^-·4-TU**
VDE (eV)	4.35	4.30	4.32
Cluster BE (kJ mol^{-1})	105.90	96.99	103.47
Vertical dipole moment (D)	7.09	6.68	7.10
Monomer dipole moment (D)[c]	4.67	4.20	4.47

[a]All binding energies are BSSE corrected.

[b] The vertical dipole moment is calculated at the MP2/6-311++G(2d,2p)/SDD level of theory.

[c] Ref [65].

3.2 Photodepletion spectra

Fig. 2 shows the photodepletion spectra of the I^-·TU clusters obtained between 3.1-5.8 eV. The three spectra are strikingly different, revealing that sulphur atom substitution impacts strongly on the excited-state. The photodepletion spectrum of I^-·2,4-TU (Fig. 2a) displays an onset at 3.2 eV and two band maxima (I and II) at 3.5 eV and 4.3 eV. A third broad band (III) is evident across the high energy region. Comparing the photodepletion spectrum of I^-·2,4-TU to the solution-phase absorption spectrum of 2,4-TU (Fig. 2d),[66] it is striking to observe that the solution-phase spectrum of the (unclustered) thiouracil is very similar to the gas-phase absorption spectrum of the cluster. The 2,4-TU solution-phase spectrum has two bands with energies and intensities close to bands I and II of the gaseous cluster spectrum.[66] This indicates that the absorption spectrum of the 2,4-TU chromophore dominates the spectrum of its iodide cluster. Band III of the photodepletion spectrum is absent from the solution-phase spectrum.

The I^-·2-TU photodepletion spectrum has an onset at approximately 3.6 eV and displays a strong absorption band (I) between 3.6-4.3 eV with λ_{max} at 4.2 eV, followed by a flatter, broad absorption region (II) between 4.6-5.6 eV. For this thionucleobase, the 2-TU monomer spectrum (Fig. 2e) does not mirror the I^-·2-TU gaseous cluster spectrum since the monomer

spectrum displays a broad region of absorption between 3.8-4.8 eV.[66] Finally, Fig. 2c shows the gas-phase photodepletion spectrum of I^-·4-TU, which displays an onset at 3.4 eV, with a first strong and broad absorption band (I) peaking at 4.02 eV. (A shoulder feature, centred close to 3.8 eV, is evident on the band's low-energy side.) A higher-lying absorption band (II) is evident from 4.76 to 5.56 eV. Intriguingly, the solution-phase spectrum of 4-TU (Fig. 2f),[66] and the I^-·4-TU cluster photodepletion spectrum are again very similar.

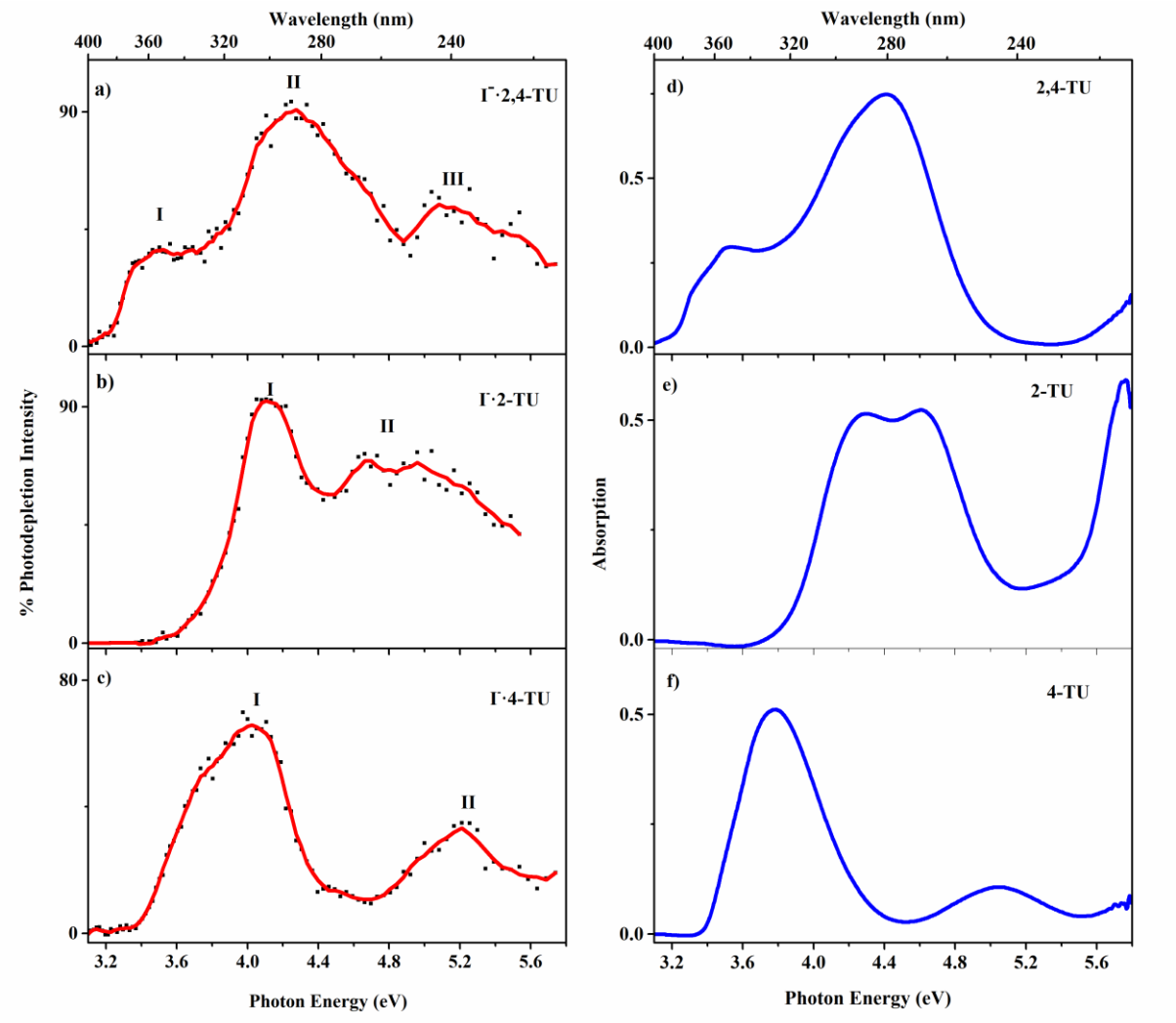

Fig. 2 Photodepletion (gas-phase absorption) spectra of a) I^-·2,4-TU, b) I^-·2-TU and c) I^-·4-TU across the range 3.1-5.7 eV. The solid line is a five-point adjacent average of the data points. Aqueous absorption spectrum of (d) 2,4-TU, (e) 2-TU and (f) 4-TU across the range 3.1 – 5.8 eV (400 – 213 nm).

3.3 Photofragmentation

3.3A Photofragment Identities

Figure 3 displays the photofragment mass spectra obtained when the I^-·TU clusters are excited at their absorption maxima, with Table 2 listing the photofragments observed and assignments. The most intense photofragment for all the clusters is the *m/z* 127 fragment, with different minor photofragments being produced by the three clusters. It is notable that all of these photofragments are low-intensity, indicating that the major channel for decay is through electron detachment.

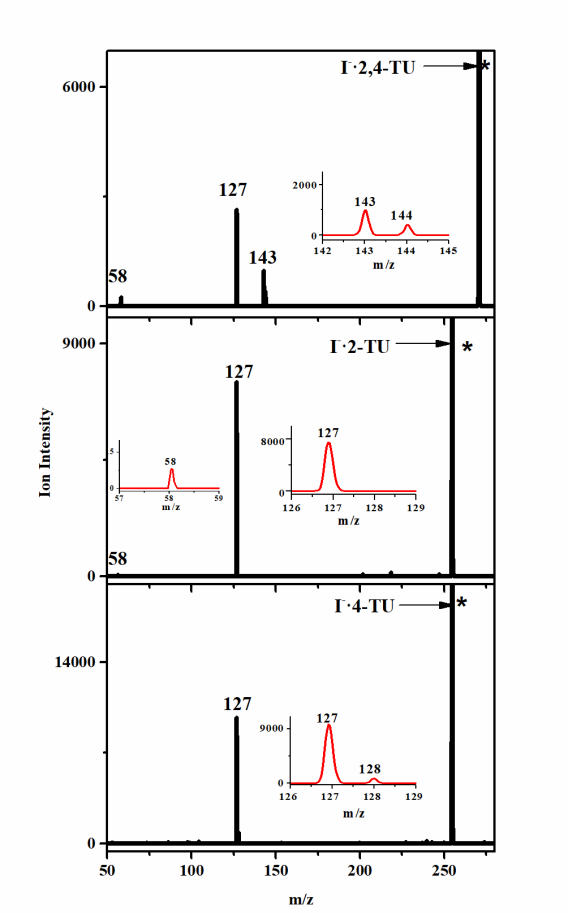

Fig. 3 Photofragment difference ($laser_{on}$-$laser_{off}$) mass spectrum of I^-·TU clusters excited at 3.5 eV (354 nm), 4.2 eV (295 nm) and 4.0 eV (310 nm) photodepletion band maxima of the individual I^-·TU clusters respectively. *Represents the precursor cluster ion signal.

For I^-·2,4-TU, the *m/z* 127 photofragment can be straightforwardly assigned to I^-, however for I^-·2-TU and I^-·4-TU, *m/z* 127 can correspond to either I^- or the deprotonated anions of 2-TU and 4-TU at the resolution of the laser-interfaced mass spectrometer.[56,57] For other iodide-nucleobase clusters we have studied,[25,26,28,29] we have observed both I^- and the respective

deprotonated nucleobase as photofragments, indicating that the *m/z* 127 peak present for I^-·2-TU and I^-·4-TU likely corresponds to a mixture of I^- and $[2\text{-TU-H}]^-$ or $[4\text{-TU-H}]^-$.[67] For I^-·2,4-TU, we do indeed observe the deprotonated anion $[2,4\text{-TU-H}]^-$ as a photofragment with *m/z* 143. Surprisingly, the molecular anion, i.e. TU^-, is observed as a photofragment from both I^-·2,4-TU and I^-·4-TU, despite the fact that the corresponding nucleobase anions have not been observed as photofragments from other iodide-nucleobase complexes.[25,26,28,29] *m/z* 58 is the final photofragment observed. This ion corresponds to SCN^-, which is one of the major dissociative electron attachment product following electron attachment to 2-TU. We note that dissociative electron detachment to 2-TU also results in production of the $[2\text{TU-H}]^-$ and S^- anions.[49-51] While $[2\text{TU-H}]^-$ appears to be produced in our experiment, S^- cannot be detected as its mass is below the cut-off of the ion trap.[56,57] (If S^- is being produced as an undetected photofragment in our experiment, its intensity should be comparable to that of SCN^-.[49-51])

Finally, the ^{34}S isotope occurs with around 4.5% intensity, and studies of this cluster isotope could clarify the ambiguity in the identities of the photofragments for the I^-·2-TU and I^-·4-TU clusters. These experiments were not, however, possible here as even using the major ^{32}S isotope clusters, the $[TU\text{-H}]^-$ photofragments were close to the detection limits of our instrument.

Table 2 Lists of photofragments with assignments observed at the Band I maxima of the I^-·TU clusters, shown with the HCD collision-induced dissociation fragments.[a]

	I^-·2,4-TU	**I^-·2-TU**	**I^-·4 TU**
Photofragments			
m/z 58	✓(SCN^-)	✓(SCN^-)	X
m/z 127	✓(I^-)	✓(I^- / $[2\text{-TU-H}]^-$)	✓(I^- / $[4\text{-TU-H}]^-$)
m/z 128	-	X	✓($[4\text{-TU-H}]^-$)
m/z 143	✓($[2,4\text{-TU-H}]^-$)	-	-
m/z 144	✓($[2,4\text{-TU}]^-$)	-	-
HCD fragments			
m/z 126.90522	✓major (I^-)	✓major (I^-)	✓major (I^-)
m/z 126.99735	-	✓minor ($[2\text{TU-H}]^-$)	✓minor ($[4\text{TU-H}]^-$)
m/z 142.97402	✓minor ($[2,4\text{-TU-H}]^-$)	-	-

[a] Section S4, ESI

3.1B Photofragment production spectra

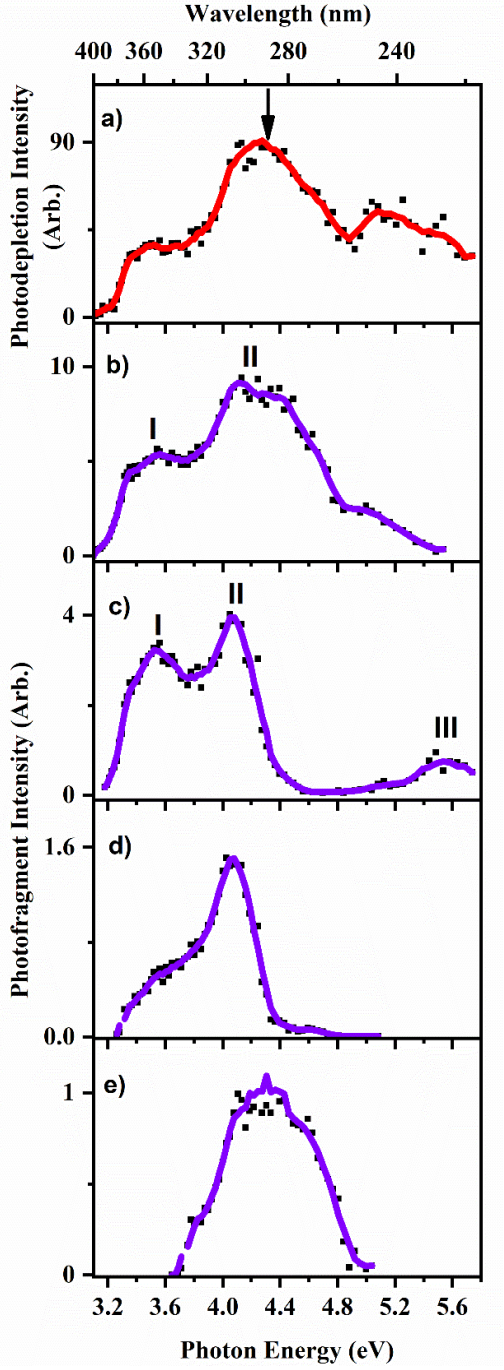

Fig. 4 a) Gas phase photodepletion spectra of I^-·2,4-TU with the b) I^-, c) $[2,4\text{-TU-H}]^-$, d) $[2,4\text{-TU}]^-$ and e) SCN^- photofragment spectra across the range 3.1-5.7 eV. (Although the photofragment intensities are arbitrary, they can be directly compared for the photofragments from this cluster, providing a measure of branching ratio.) The solid line is a five-point adjacent average of the data points, while the arrow represents the calculated VDE.

Fig 4 displays the photofragment production spectra associated with $I^-\cdot$2,4-TU, shown with the photodepletion spectrum for comparison. I^- (Fig. 4b) is the most intense photofragment, and is produced across the entire photodepletion spectrum with peaks in production through the band I and band II maxima. $[2,4\text{-TU-H}]^-$ is the second most intense fragment (Fig. 4c). This photofragment's production is also maximised through the band I and II maxima, although its production drops sharply after the band II peak. The $[2,4\text{-TU}]^-$ fragment production profile (Fig. 4d) is similar to that of $[2,4\text{-TU-H}]^-$ through the band II region, although its production through the band I region is somewhat lower. Finally, the production spectrum of the very low intensity photofragment, SCN^-, is shown in Fig. 4e. This photofragment displays a distinctive production profile, with an onset at 3.65 eV, and production across a region that peaks just above the band II maximum.

The *m/z* 127 (I^- and $[2\text{-TU-H}]^-$) photofragment action spectrum produced from $I^-\cdot$2-TU across the region 3.1-5.7 eV is presented with the photodepletion spectrum for comparison in Fig. 5. The photofragment production spectrum peaks at ~ 4.04 eV (I) and ~ 4.6 eV (II), before tailing off to higher energies.

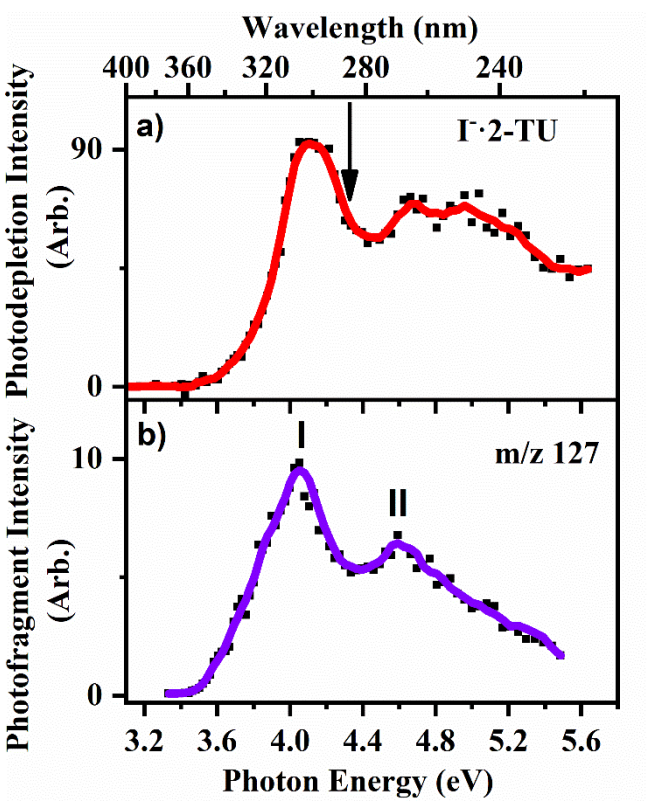

Fig. 5 a) Gas phase photodepletion spectrum of $I^-\cdot$2-TU and b) the *m/z* 127 photofragment action spectrum, across the range 3.1-5.7 eV. The solid line is a five-point adjacent average of

the data points, while the arrow represents the calculated VDE.

Fig. 6 displays the photofragment production spectra for I^-·4-TU, along with the photodepletion spectrum. The *m/z* 127 (I^- and $[4\text{-TU-H}]^-$) photofragment spectrum peaks at the band I maximum of 3.81 eV, and again with lower intensity (II) around 5.1 eV. The *m/z* 128 molecular ion photofragment, $[4\text{-TU}]^-$ (Fig. 6c), is produced only within the band I region, with an onset at 3.5 eV. Its production spectrum displays a shoulder at ~3.6 eV prior to a well resolved peak at 4.1 eV, with intensity that falls away sharply after the peak.

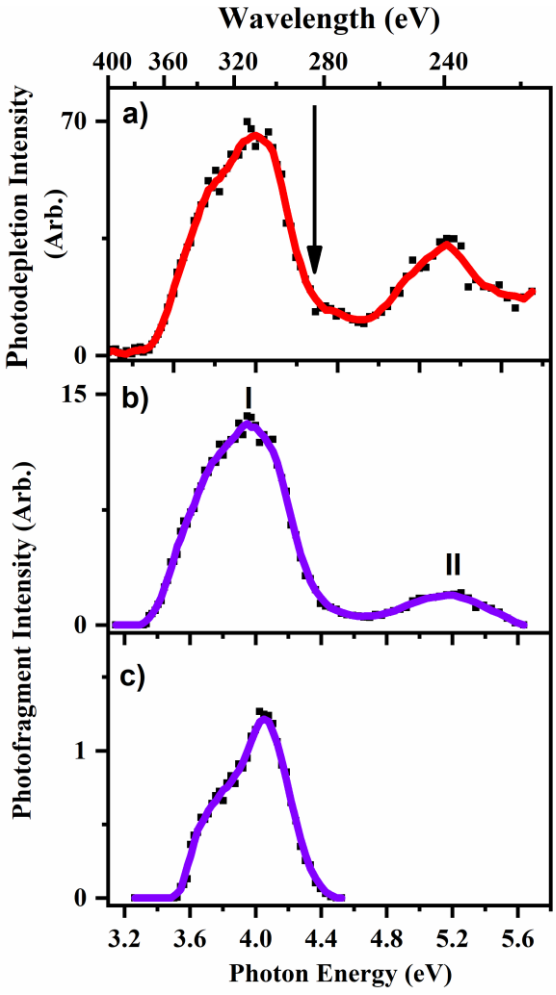

Fig. 6 a) Gas phase photodepletion spectrum of the I^-·4-TU cluster and photofragment action spectra of b) *m/z* 127 and c) $[4\text{-TU}]^-$ across the range 3.1-5.7 eV. (Although the photofragment intensities are arbitrary, they can be directly compared for the photofragments from this cluster, providing a measure of branching ratio.) The solid line is a five-point adjacent average of data point while the arrow represents the calculated VDE.

4 Discussion

4.1 Assignment of the observed excited states from the photodepletion spectra

The solution-phase spectrum of 2,4-TU displays two peaks over the 3.2-5.7 eV spectral region, with λ_{max} at 3.45 eV and 4.55 eV.[66] These peaks occur at similar energies to bands I and II of the I^-·2,4-TU spectrum, indicating that the cluster excited states in these regions are associated with π-π^* localized transitions of the 2,4-TU moiety. In other iodide-molecule clusters, dipole-bound excited states have been observed in the region of the VDE.[25,26,28,29] We anticipate that the VDE of I^-·2,4-TU should occur around 4.1 eV, so a dipole-bound excited state is expected to occur for the cluster around this energy. The photodepletion spectrum does not display the sharp fall-off in photodepletion intensity that is typically observed at the high-energy edge of the dipole-bound excited state,[68,69] so it is not possible to conclude that the dipole-bound excited state exists for I^-·2,4-TU from its photodepletion spectrum. This is a situation we have observed in previous studies of iodide-pyrimidine clusters,[25,26] and we will return to this point when we discuss the cluster's photofragment production spectra below. Band III of the photodepletion spectrum does not correlate with any prominent transitions of the 2,4-TU chromophore, and since this spectral region lies above the expected VDE of the cluster, it can be assigned to direct electron detachment (Fig. S5, ESI).[25,26]

In contrast to I^-·2,4-TU, the I^-·2-TU photodepletion spectrum does not display the same features as the solution-phase spectrum of 2-TU, which is characterised by a pair of partially-resolved bands with λ_{max} of 4.2 and 4.7 eV.[66] The I^-·2-TU spectrum displays a strong photodepletion onset around 3.6 eV, peaking at 4.1 eV, in the vicinity of the predicted VDE (band I). The near-threshold band is followed by a rather flat region of photodepletion between 4.6-5.6 eV. This spectral profile is typical of a number of iodide ion-polar molecule complexes,[25,26] where the band I feature has been assigned to a dipole-bound excited state followed by a region of direct electron detachment.[70,71] This leads us to assign band I to a near-threshold dipole-bound excited state of I^-·2-TU. There are no strong signatures of π-π^* localized 2-TU excited states evident on the photodepletion spectrum. (We note that two features can tentatively be seen at ~ 4.5 and 5 eV in the photodepletion spectrum, which could correspond to the π-π^* 2-TU excitations. However, they can certainly not be described as prominent spectral features, and are only just visible above the electron detachment background.)

The solution-phase spectrum of 4-TU displays a very strong band with λ_{max} at ~3.8 eV, followed by a lower-intensity band with λ_{max} at ~5.0 eV.[66] These features are associated with π-π^* transitions of the 4-TU chromophore.[66] The photodepletion spectrum of I^-·4-TU displays a band peaking at ~4.1 eV (band I), followed by a lower-intensity band (II) at 5.2 eV. Band I could either be associated with a dipole-bound excited state or with excitation of the lower-energy strong 4-TU π-π^* transition. It is probable that contributions from both of these very distinctive excited states are present in this excitation region as will be discussed further below. Band II can be assigned to excitation of the higher-energy π-π^* transition in the cluster.

Having performed a preliminary assignment of the excited states evident in the photodepletion spectra of the I^-·TU clusters, it is now useful to compare the experimental spectra to TDDFT generated spectra (Fig. 7) The TDDFT calculations are expected to predict π-π* nucleobase-localized transitions reasonably well, but are not expected to accurately predict dipole-bound excited states. Comparing the calculated and experimental spectra, there is good agreement for I^-·2,4-TU and I^-·4-TU, while the I^-·2-TU calculated spectrum does not closely resemble the photodepletion spectrum. The good agreement observed for I^-·2,4-TU and I^-·4-TU reflects the fact that the experimental spectra for these complexes are dominated by the π-π* nucleobase-localized transitions.

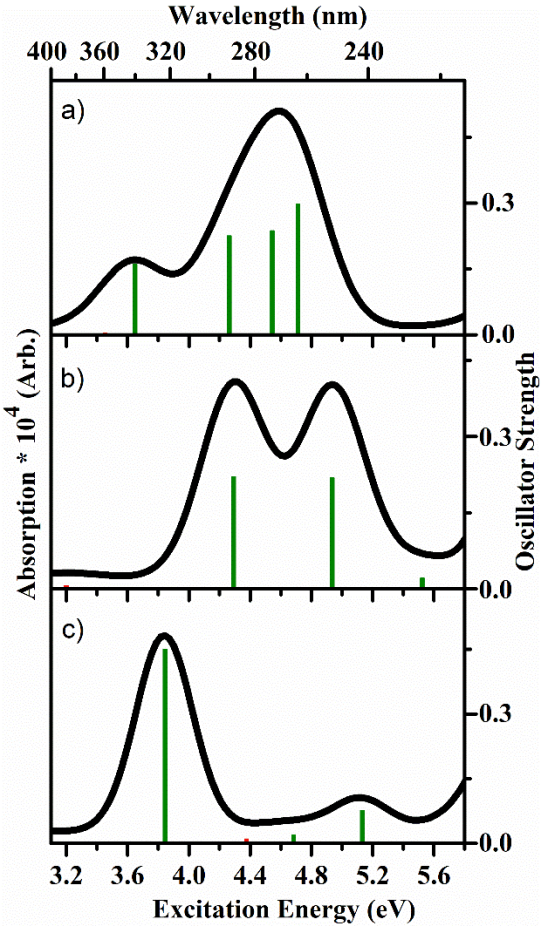

Fig. 7 TDDFT (M062X/ DEF2SVP) excitation spectra of a) I^-·2,4-TU, b) I^-·2-TU and c) I^-·4-TU clusters. The oscillator strengths on the y axis of individual transitions ≥ 0.005 are shown by vertical bars while the full line spectrum is a convolution of the calculated spectrum with Gaussian function (0.25 eV HWHM). (The red line represents transitions from an iodide p-orbital and the green lines represent transitions from thiouracil π orbitals.)

Finally, it is of interest to consider whether the two spin-orbit states of the iodine atom in the photodetached clusters contribute to the photodepletion spectra. Although direct detachment to the upper $^2P_{1/2}$ neutral state around 5 eV has been observed for some iodide ion pyrimidine complexes (I^-·U and I^-·T) via photoelectron spectroscopy,[25,26] photodepletion spectra did not clearly show the upper spin-orbit dipole-bound state.[72] The I^-·TU complexes behaviour appears to be in line with that of the previously studied iodide ion pyrimidine complexes (I^-·U and I^-·T), in that the upper spin orbit dipole-bound excited state is not clearly evident on the photodepletion spectra. (It would be expected to appear around 5.1 eV.) We conclude that excitation to the upper spin-orbit state is occurring with relatively low cross section.[26]

4.2 Photofragment production

Two general mechanisms are associated with production of ionic photofragments in clusters such as the I^-·TU complexes studied here. The first group correspond to various intracluster electron-transfer processes, including events that follow dipole-bound excited state formation, ejection of a low energy electron from I^- that then undergoes electron scattering from the thionucleobase, or straightforward charge transfer from I^- to the thionucleobase valence orbitals.[27] This group of processes are expected to result in production of either the dipole-bound anion of the thionucleobase through direct fragmentation of the dipole-bound excited state, or of the deprotonated thionucleobase since this is the most intense fragment expected when the thionucleobase captures a free electron.

The second type of photofragmentation follows electronic excitation that is largely localized on the nucleobase chromophore. Native nucleobases are known for their propensity to decay back to the electronic ground state following UV excitation and then lose excess energy by thermal dissipation.[73] In an anion-nucleobase complex, when electronic relaxation of a nucleobase centred excited state results in a return to the electronic ground state, followed by thermal fragmentation, we expect to observe the same ionic fragments that would be produced upon low-energy CID.[74,75] On conducting CID experiments for the I^-·TU clusters, we observed production of the iodide ion and the respective deprotonated thionucleobase (Section S4, ESI). Simultaneous production of I^- and $[TU-H]^-$ as photofragments could therefore be interpreted as arising from ultrafast decay of a thionucleobase-centred excited state. There are two important points however to note. Firstly, thionucleobases are known to exhibit much less efficient ultrafast decay than native nucleobases, potentially meaning that the I^-·TU excited states could be significantly longer-lived than those of iodide-native nucleobases.[37,38,42,45-48] Secondly, even in the iodide-native nucleobase clusters, excited states (both dipole-bound and nucleobase localized) have been observed to decay with long lifetimes, consistent with internal conversion to the ground electronic state followed by evaporation of I^- and the deprotonated nucleobase.[25,26] Ultimately, analysis of the production profile of individual photofragments is crucial in assigning the nature of the excited state involved in generating specific photoproducts.

For I^-·2-TU, the *m/z* 127 (I^- / $[2-TU-H]^-$) photofragment profile is very like that of the

comparable fragments for the iodide pyrimidine complexes,[25,26] suggesting that similar photofragmentation mechanisms are present, *i.e.* intracluster electron transfer dominates in the near threshold region, while 2TU-centred excitations dominate close to the band II nucleobase localized π-π* transition. In I^-·4-TU, the *m/z* 127 (I^- / $[4\text{-TU-H}]^-$) photofragment displays a similar profile to the *m/z* 127 photofragment of the I^-·2-TU cluster, indicating the presence of similar excited states and decay processes. However, there is a notable difference in the profile of the second photofragment, the molecular anion, $[4\text{-TU}]^-$. Its production profile displays a very sharp falloff in intensity above the expected VDE, suggesting that this photofragment is formed directly from decay of a precursor dipole-bound excited state. Our experiment does not allow us to measure whether this anion is a dipole-bound or valence anion, although time-resolved photoelectron spectroscopy could be applied in future experiments to clarify this.[27,71]

I^-·2,4-TU provides the richest photofragmentation pattern. The I^- ion is produced across most of the scanned region with a profile that largely resembles that of photodepletion. (I^- production decreases > 5.0 eV, but this is consistent with electron detachment increasingly dominating at high excitation energies). The similar appearance of the I^- production and the photodepletion spectrum indicates that I^- is being produced from decay of all of the excited states present for the cluster, behaviour that again mirrors that seen for the iodide-pyrimidine complexes.[25,26] As for the $[4\text{-TU}]^-$ photofragment from I^-·4-TU, the $[2,4\text{-TU}]^-$ molecular anion photofragment from I^-·2,4-TU displays a production profile indicative of production through a dipole-bound excited state in the region of the VDE, with a sharp fall in intensity around the expected VDE.[30] Indeed, this photofragment's production profile can be directly associated with a dipole-bound excited state, and thus confirms that such a state is present in this region for I^-·2,4-TU.

The profile for production of $[2,4\text{-TU-H}]^-$ is similar to that of the I^- photofragment in the lower energy region of the spectrum, again mirroring the behaviour of the iodide-pyrimidine complexes.[25,26] However, its intensity drops sharply above 4.2 eV, on the high-energy edge of the dipole-bound excited state. This leads us to conclude that the dipole-bound excited state decays with production of both $[2,4\text{-TU}]^-$ and $[2,4\text{-TU-H}]^-$. (Low level production of the $[2,4\text{-TU-H}]^-$ photofragment is observed in the region around 5.2 eV, possibly associated with decay of the upper spin-orbit excited state). We note that the $[2,4\text{-TU}]^-$ fragment is produced considerably less strongly through the lower energy band I region than $[2,4\text{-TU-H}]^-$. Indeed, what is surprising is that $[2,4\text{-TU}]^-$ is seen at all in this region, since band I corresponds to a

thionucleobase localized excited state. The simplest explanation of the proximity of the thionucleobase band I excited state with the cluster dipole-bound excited state is resulting in strong coupling of these two very distinctive excited states.

The SCN^- photofragment profile from I^-·2,4-TU is distinctive compared to the other photofragments, with production limited to the region between 3.6 eV-4.9 eV. It is notable that SCN^- production does not follow the dipole-bound excited state profile established by the $[2,4\text{-TU}]^-$ photofragment, allowing us to conclude that this fragment is not a biproduct of electron transfer onto 2,4-TU. This spectral region corresponds to the more intense π-π* localized transition of 2,4-TU. It is very notable that $[2,4\text{-TU-H}]^-$ is not being produced though this region. This suggests that the chromophore-centred excited state accessed in this region does not decay directly back to the ground state with statistical evaporation of the primary fragment pair, but instead evolves to eject SCN^- as a dissociative photoproduct. This behaviour is in line with the known distinctive behaviour of thionucleobases compared to native nucleobases.[53]

5 Further Discussion

In most respects, the photophysics and photochemistry of the I^-·TU complexes closely resemble those of the iodide-pyrimidine complexes studied previously.[25,26] Photoexcitation predominantly results in electron detachment (likely via autodetachment following electronic excitation of the cluster), with ionic fragmentation representing only a minor decay pathway. However, two aspects of the results merit further discussion.

The first relates to the identities of the $[4\text{-TU}]^-$ and $[2,4\text{-TU}]^-$ anions produced following photoexcitation of I^-·4-TU and I^-·2,4-TU, respectively. Photoelectron spectroscopy of $[4\text{-TU}]^-$ and $[2,4\text{-TU}]^-$ was conducted by Bowen and co-workers, with the results compared to the uracil molecular anion, U^-.[54] While U^- was identified as a dipole-bound anion, both $[4\text{-TU}]^-$ and $[2,4\text{-TU}]^-$ were found to be valence anions. Accompanying theoretical calculations revealed that $[4\text{-TU}]^-$ and $[2,4\text{-TU}]^-$ are considerably more stable as valence anions than both $[2\text{-TU}]^-$ and U^-, with only $[4\text{-TU}]^-$ and $[2,4\text{-TU}]^-$ displaying positive vertical electron affinities.[55] The behaviour of uracil mirrors that of the other canonical nucleobases, since their valence anions have generally been elusive in the gas-phase (except in delicate Rydberg electron transfer

experiments),[76] likely due to their low electron affinities.[77] Indeed, U^- was not observed as a photofragment in photoexcitation of I^-·U,[25] and it appears that the I^-·2-TU complex studied in this work is displaying very similar behaviour, with 2-TU^- not being observed as a photofragment. Therefore, in our experiments on I^-·4-TU and I^-·2,4-TU, initial photoexcitation in the VDE region accesses a dipole-bound excited state, which decays with formation of $[4\text{-TU}]^-$ and $[2,4\text{-TU}]^-$ as stable valence molecular anions. For I^-·2-TU, photoexcitation in the near threshold region again accesses a dipole-bound excited state, but the ultimate photoproduct is $[2\text{-TU-H}]^-$ as the valence-bound form of $[2\text{-TU}]^-$ is not sufficiently stable, so that the dissociative electron attachment product is the end product.

In the context of the above discussion, it is notable that I^-·2-TU can also be considered to be the "odd man out" compared to I^-·4-TU and I^-·2,4-TU in relation to the general profile of the photodepletion (gas-phase absorption) spectra. The photodepletion spectra of I^-·4-TU and I^-·2,4-TU both strongly resemble the intrinsic absorption spectra of the uncomplexed nucleobases, i.e. the nucleobase localized π-π^* transitions dominate these spectra. Intriguingly, this is not the case for I^-·2-TU. Comparing the calculated properties of the clusters (Table 1) reveals that I^-·2-TU has a weaker cluster binding energy and vertical dipole moment than the other two clusters, due to the relatively lower dipole moment of 2-TU. An intriguing possibility is that the stronger dipole moments of 4-TU and 2,4-TU are enhancing the coupling of the electron detachment continuum to nucleobase-centred transitions. Current understanding of the physics of how molecular excited states couple to the electron detachment continuum is an area of emerging interest,[78-81] and further theoretical insight is urgently needed to better understand the photophysics and electron dynamics.[81] The thionucleobases provide a useful series of molecules for extending the current studies given that the molecular dipole changes significantly with derivatization.

Conflicts of Interest

There are no conflicts to declare.

Author Contributions

Conceptualization, C.E.H.D.; formal analysis, K.O.U.; investigation, K.O.U.; resources, C.E.H.D.; data curation, K.O.U.; writing—original draft preparation, K.O.U.; writing—review

and editing, C.E.H.D, and K.O.U.; supervision, C.E.H.D.; funding acquisition, C.E.H.D.

Acknowledgements

Acknowledgment is made to the donors of the American Chemical Society Petroleum Research Fund for partial support of this research, through the award of grant ACS PRF 56174-ND6. We thank the University of York and the Department of Chemistry for funding the Horizon OPO laser system, and York Advanced Computing Cluster (YARCC) for access to computational resources. K.O.U thanks the Tetfund for the award of a PhD studentship and the Department of Chemistry's Tony Wild fund for additional support. We also acknowledge the facilities of the York Centre of Excellence in Mass Spectrometry, which was created thanks to a major capital investment through Science City York, supported by Yorkshire Forward with funds from the Northern Way Initiative, and subsequently received additional support from the EPSRC.

References

1. S. M. Pimblott and J. A. LaVerne, Radiat. Phys. Chem., 2007, **76**, 1244 -1247.
2. L. Sanche**,** Radiat**.** Phys. Chem., 1989, **34**, 15.
3. B. Boudaiffa, P. Cloutier, D. Hunting, M. A. Huels, and L. Sanche, Science, 2000, **287**, 1658 – 1660.
4. L. Sanche, Eur. Phys. J. D, 2005, **35**, 367 -390
5. J. K. Wolken and F. Turecek, J. Phys. Chem. A ,2001, **105,** 8352-8360.
6. S. G. Ray, S. S. Daube, and R. Naaman, Proc. Natl. Acad. Sci. U.S.A, 2005, **102**, 15-19.
7. H. Abdoul-Carime, S. Gohlke, and E. Illenberger, Phys. Rev. Lett., 2004, **92**, 168103.
8. J. Simons, Acc. Chem. Res., 2006, **39**, 772- 779
9. J. D. Gu, J. Leszczynski, and H. F. Schaefer, Chem. Rev., 2012, **112**, 5603- 5640
10. H.Y. Chen, P.Y. Yang, H. F. Chen, C. L. Kao, and L. W. Liao, J. Phys. Chem. B, 2014, **118**, 11137-11144.
11. X. Pan and L. Sanche, Chem. Phys. Lett., 2006, **421**, 404-408.
12. G. Z. Zhu, L. F. Cheung, Y. Liu, C. H. Qan, L. S. Wang, J. Phys. Chem. Lett. 2019, **10**, 4339-4344.
13. Y. Dong, Y. Gao, W. Liu, T. Gao, Y. Zheng and L. Sanche , J. Phys. Chem. Lett., 2019. **10** , 2985-2990
14. S. Denifl, S. Ptasinska, G. Hanel, B. Gstir, M. Probst, P. Scheier and T. D. Mark , J. Chem. Phys., 2004, **120** ,6557-6565
15. J. Ameixa, E. ArthurBaidoo, R. Meißner, S.Makurat, W. Kozak, K. Butowska, F. Ferreira da Silva, J. Rak and S. Denifl , J. Chem. Phys., 2018, **149** , 164307.
16. J. K. Wolken and F. Turecek , J. Am. Chem. Soc., 2001, **123** , 5804-5805

17. J. H. Hendricks, S. A. Lyapustina, H. L. de Clercq, J. T. Snodgrass and K. H. Bowen, J. Chem. Phys., 1996, **104** , 7788-7791 .
18. H. Y. Chen, P. Y. Yang, H. F. Chen, C. L. Kao and L. W. Liao, J. Phys. Chem. B., 2014, **118** , 11137-11144.
19. M. Haranczyk and M. Gutowski, J. Am. Chem. Soc.,2005, **127** , 699-706.
20. M. A. Fennimore and S. Matsika, J. Phys. Chem. A.. 2018, **122** , 4048-4057.
21. M. A. Yandell, S. B. King, and D. M. Neumark, J. Am. Chem. Soc., 2013, **135**, 2128-2131.
22. S. B. King, M. A. Yandell, and D. M. Neumark, Faraday Disscuss.,2013, **163**, 59-72.
23. S. B. King, M. A. Yandell, A. B. Stephansen, and D. M. Neumark, J. Chem. Phys.,2014 **141**, 224310.
24. S. B. King, A. B. Stephansen, Y. Yokoi, M. A. Yandell, A. Kunin, T. Takayanagi, and D. M. Neumark, J. Chem. Phys., 2015, **143**, 024313
25. W. Li, K. Alice, E. Matthews, N. Yoshikawa, C. E. H. Dessent, and D. M. Neumark, J. Chem. Phys., 2016, **145**, 044319.
26. E. Matthews, R. Cercola, G. Mensa-Bonsu, D. M. Neumark, and C. E. H. Dessent, J. Chem. Phys., 2018, **148**, 084304.
27. A. Kunin, and D. M. Neumark, Phys. Chem. Chem. Phys., 2019, **21**, 7239-7255.
28. R. Cercola, E. Matthews, and C.E.H. Dessent, Mol. Phys., 2019, **117**, 3001-3010.
29. R. Cercola, K.O Uleanya, and C.E.H. Dessent, 2019, Mol. Phys., **118**, e1679402
30. C. E. H. Dessent, J. Kim, and M. A. Johnson, Faraday Discuss., 2000, **115**, 395-406.
31. M. Pollum, S. Jockusch, C. E. Crespo-Hernández, J. Am. Chem. Soc., 2014, **136**, 17930–17933.
32. O. Reelfs, P. Karran, A. R Young, Photochem. Photobiol. Sci., 2012, **11**, 148–154.

33. G. Trigiante and Y. Z. Xu, Photodynamic Therapy: Fundamentals, Applications and Health Outcomes, Hugo, A.G., Ed., Nova Science Publishers: Hauppauge, NJ, USA, 2015.
34. K. M. Farrell, M. M. Brister, M. Pittelkow, T. I. Sølling and C. E. Crespo-Hernández, J. Am. Chem. Soc. 2018, **140**, 11214–11218.
35. R. Borrego-Varillas, D. C. Teles-Ferreira, A. Nenov, I. Conti, L. Ganzer, C. Manzoni, M. Garavelli, A. Maria de Paula and G. J. Cerullo, J. Am. Chem. Soc., 2018, **140**, 16087–16093.
36. H. Yu, J. A. Sanchez-Rodriguez, M. Pollum, C. E. Crespo-Hernández, S. Mai, P. Marquetand, L. González and S. Ullrich, Phys. Chem. Chem. Phys. 2016, **18**, 20168–20176.
37. J. A Sánchez-Rodríguez, A. Mohamadzade, S. Mai, B. Ashwood, M. Pollum, P. Marquetand, L. González, C. E. Crespo-Hernández and S. Ullrich, Phys. Chem. Chem. Phys. 2017, **19**, 19756–19766.
38. M. Pollum, S. Jockusch and C. E. Crespo-Hernández, Phys. Chem. Chem. Phys., 2015, **17**, 27851–27861.
39. V. Vendrell-Criado, J.A. Sáez, V. Lhiaubet-Vallet, M. C. Cuquerella and M. A. Miranda, Photochem. Photobiol. Sci., 2013, **12**, 1460 -1465
40. Y. Harada, T. Suzuki, T. Ichimura and Y. Z. Xu, J. Phys. Chem. B, 2007, **111**, 5518–5524.
41. L. Martínez-Fernández, G. Granucci, M. Pollum, C. E. Crespo-Hernández, M. Persico and I. Corral, Chem. A Eur. J., 2017, **23**, 2619–2627.
42. D. Koyama, M. J. Milner and A. J. Orr-Ewing, J. Phys. Chem. B, 2017, **121**, 9274–9280.

43. L. Martínez-Fernández, L. González and I. Corral, Chem. Commun., 2012, **48**, 2134-2136.
44. G. Cui and W. Fang, J. Chem. Phys. 2013, **138**, 044315.
45. J. P. Gobbo and A. C. Borin, Comput. Theor. Chem., 2014, 1040–1041, 195–201.
46. S. Mai, P. Marquetand and L. A González, J. Phys. Chem. A, 2015, **119**, 9524–9533.
47. S. Mai, P. Marquetand and L. González, J. Phys. Chem. Lett., 2016, **7**, 1978–1983.
48. D. C. Teles-Ferreira, I. Conti, R. Borrego-Varillas, A. Nenov, I. H. M. Van Stokkum, L. Ganzer, C. Manzoni, A. M. Paula, G. Cerullo and M. A. Garavelli, Chem. A Eur. J. 2020, **26**, 336–343.
49. J. Kopyra, H. Abdoul-Carime, F. Kossoskic and M. T. do N. Varella, Phys. Chem. Chem. Phys., 2014, **16**, 25054-25061.
50. J. Kopyra and H. Abdoul-Carime, J. Chem. Phys., 2016, 144, 034306.
51. J. Kopyra, K.K. Kopyra, H. Abdoul-Carime and D. Branowska, J. Chem. Phys., 2018, **148**, 234301.
52. S. Taras-Goslinska and J. Bobrowski., Molecules, 2019, **24**, 4402.
53. K. O. Uleanya, R. Cercola, M. Nikolova, E. Matthews, N. G. K. Wong and C E. H. Dessent, Molecules, 2020, **25**, 3157.
54. X. Li, J. Chen, and K. H. Bowen, J. Chem. Phys., 2011, **134**, 074304.
55. O. Dolgounitcheva, V. G. Zakrzewski, and J. V. Ortiz, J. Chem. Phys., 2011, **134**, 074305.
56. E. Matthews, A. Sen, N. Yoshikawa, E. Bergstrom, and C. E. H. Dessent, Phys. Chem. Chem. Phys., 2016, **18**, 15143.
57. A. Sen, T. F. M. Luxford, N. Yoshikawa, and C. E. H. Dessent, Phys. Chem. Chem. Phys., 2014, **16**, 15490.

58. P. Jedrychowski, E. L. Huttlin, W. Haas, M. E. Sowa, R. Rad and S.P Gygi, Mol. Cell. Proteomics, 2011, **10**, M111.009910.

59. J.V Olsen, B. Macek, O. Lange, A. Makarov, S. Horning and M. Mann, Nat. Methods, 2007, **4**, 709–712.

60. R. Cercola, E. Matthews, C. E. H. Dessent, J. Phys. Chem. B, 2017, **121**, 5553–5561.

61. M. J. Frisch, G. W. Trucks, H. B. Schlegel, G. E. Scuseria, M. A. Robb, J. R. Cheeseman, G. Scalmani, V. Barone, B. Mennucci, G. A. Petersson, H. Nakatsuji, M. Caricato, X. Li, H. P. Hratchian, A. F. Izmaylov, J. Bloino, G. Zheng, J. L. Sonnenberg, M. Hada, M. Ehara, K. Toyota, R. Fukuda, J. Hasegawa, M. Ishida, T. Nakajima, Y. Honda, O. Kitao, H. Nakai, T. Vreven, J. A. Montgomery Jr., J. E. Peralta, F. Ogliaro, M. J. Bearpark, J. Heyd, E. N. Brothers, K. N. Kudin, V. N. Staroverov, R. Kobayashi, J. Normand, K. Raghavachari, A. P. Rendell, J. C. Burant, S. S. Iyengar, J. Tomasi, M. Cossi, N. Rega, N. J. Millam, M. Klene, J. E. Knox, J. B. Cross, V. Bakken, C. Adamo, J. Jaramillo, R. Gomperts, R. E. Stratmann, O. M Yazyev, A. J. Austin, R. Cammi, C. Pomelli, J. W. Ochterski, R. L. Martin, K. Morokuma, V. G. Zakrzewski, G. A. Voth, P. Salvador, J. J. Dannenberg, S. Dapprich, A. D. Daniels, O¨. Farkas, J. B. Foresman, J. V. Ortiz, J. Cioslowski and D. J. Fox, Gaussian 09, Revision D.01, Gaussian, Inc., Wallingford, CT, 2009.

62. W. R. Garrett, J. Chem. Phys., 1982, **77**, 3666-3673.

63. O. H. Crawford and W. R. Garrett, J. Chem. Phys.,1977, **66**, 4968-4970.

64. O. H. Crawford, Mol. Phys.,1971, **20**, 585-591.

65. W. C. Schneider and I. F. Halverstadt, J. Am. Chem. Soc., 1948, **70**, 2626-2631.

66. S. Arslancan, L. Martínez-Fernández, and I. Corral, Molecules, 2017, **22**, 998.

67. We note that at higher mass resolution, the masses are I^- = 126.90522 and $(2\text{-TU-H})^-$ or $(4\text{-TU-H})^-$ = 126.99735. These masses can be distinguished in the Orbitrap Fusion

Tribrid mass spectrometer available in our research group. Photofragmentation is not possible in this mass spectrometer, but higher-collisional energy dissociation (HCD) was performed on the clusters. We observed both I^- and $(TU-H)^-$ as fragments in these experiments (Fig. S4, ESI) for both $I^-\cdot$2-TU and $I^-\cdot$4-TU with an intensity ratio of ~ 90% to 10%, respectively. This shows that the electronic ground states of the $I^-\cdot$2-TU and $I^-\cdot$4-TU clusters do fragment with production of both I^- and $(TU-H)^-$.

68. E. Matthews and C. E. H. Dessent, J. Phys. Chem. Lett., 2018, **9**, 6124–6130.
69. A. J. A. Harvey, N. Yoshikawa, J. G. Wang, and C. E. H. Dessent, J. Chem. Phys., 2015, **143**, 101103.
70. A. Henley and H. H. Fielding, Int. Rev. Phys. Chem. 2019, **38**, 1-34.
71. C. S. Anstoter, J. N. Bull, and J. R. R. Verlet, 2016, **35**, 509-538.
72. F. Mbaiwa, D. Dao, N. Holtgrewe, J. Lasinski, and R. Mabbs, J. Chem. Phys., 2012, **136**, 114303.
73. C. E. Crespo Hernandez, B. Cohen, P.M. Hare and B. Kohler, Chem. Rev., 2004, **104**, 1977–2020.
74. A. Sen and C.E.H. Dessent, J. Phys. Chem. Lett., 2014, **5**, 3281-3285.
75. A. Sen and C.E.H. Dessent, J. Chem. Phys., 2014, **141**, 241101.
76. C. Desfrançois, H. Abdoul-Carime, N. Khelifa and J. P. Schermann, Phys. Rev. Lett., 1994,**73**, 2436–2439.
77. P. Skurski, M. Gutowski, and J. Simons, Int. J. Quantum Chem., 2000, **80**, 1024-1038.
78. S. Daly, M. Pornini, F. Rosu, and V. Gabelica, Farad. Discuss. 2019, **217**, 361-382.
79. A. Sen, G. L. Hou, X. B. Wang, C. E. H. Dessent, J. Phys. Chem. B, 2015, **119**, 11626-11631.
80. A. Sen, E. M. Matthews, G. L. Hou, X. B. Wang, and C. E. H. Dessent, J. Chem. Phys. 2015, **143**, 11B608-1.

81. M. Ahmed et al. Farad. Discuss. 2019, **217**, 138-171.

Electronic Supplementary Information

Investigating the Mapping of Chromophore Excitations onto the Electron Detachment Spectrum: Photodissociation Spectroscopy of Iodide Ion-Thiouracil Clusters

Kelechi O. Uleanya and Caroline E. H. Dessent*
Department of Chemistry, University of York, Heslington, York YO10 5DD, UK.

* Corresponding author: caroline.dessent@york.ac.uk

S1: DFT calculations of the tautomers of the I^- ·TU clusters

The structures of the I^- ·TU clusters (TU = 2,4-thiouracil, 2-thiouracil and 4-thiouracil) clusters were optimised from multiple starting structures mainly from tautomers obtained by Andrzej Les and Ludwik Adamowicz.[1] The lowest energy structure of each I^- ·TU cluster are presented in Tables S1, S2 and S3 respectively. For each I^- ·TU cluster, the keto form was found to produce the lowest energy structure T1.

Table S1 Calculated structures and relative electronic energies of the tautomers 2,4-thiouracil iodide (I^-·2,4-TU) clusters. Structures were calculated at the B3LYP/6-311++G(2d,2p) level, 6-311G(d,p)/SDD on I (see main text for details).Energies are zero-point energy corrected.

Tautomer	Energy (kJ/mol)	Tautomer	Energy (kJ/mol)
T1 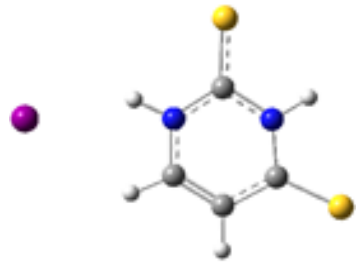	0.0	T4 	60.31
T2 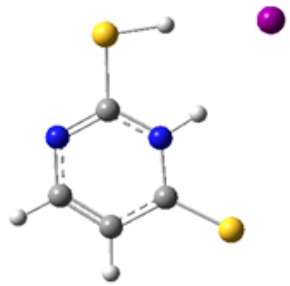	39.62	T5 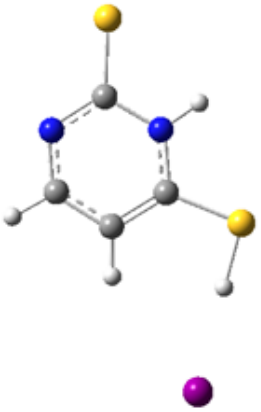	55.47
T3 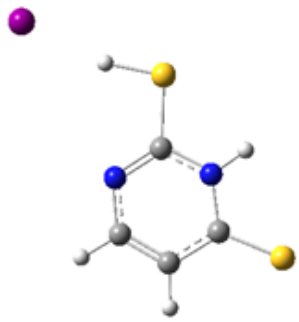	60.52	T6 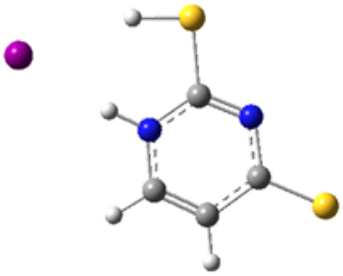	41.33

Table S2 Calculated structures and relative electronic energies of the tautomers 2-thiouracil iodide (I^-·2-TU) clusters. Structures were calculated at the B3LYP/6-311++G(2d,2p) level, 6-311G(d,p)/SDD on I (see main text for details).Energies are zero-point energy corrected

Tautomer	Energy (kJ/mol)	Tautomer	Energy (kJ/mol)
T1 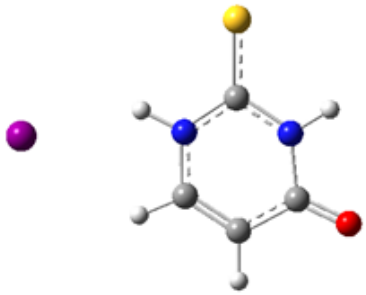	0.0	T4 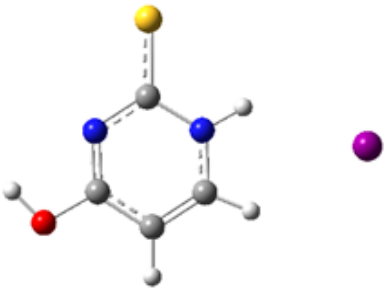	60.22
T2 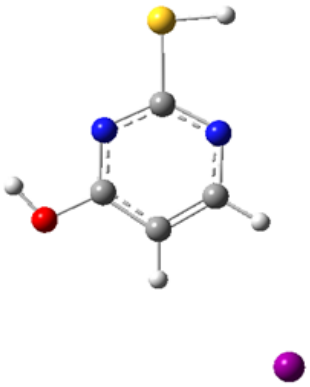	70.25	T5 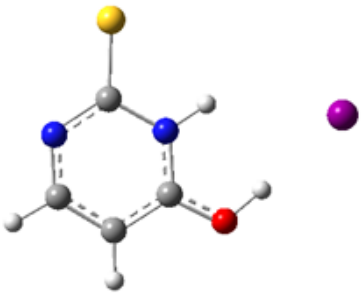	44.88
T3 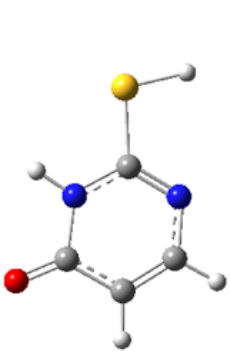	66.73	T6 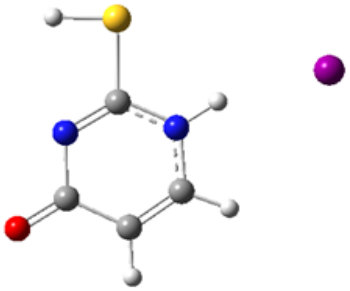	55.98

Table S3 Calculated structures and relative electronic energies of the tautomers 4-thiouracil iodide (I^-·4-TU) clusters. Structures were calculated at the B3LYP/6-311++G(2d,2p) level, 6-311G(d,p)/SDD on I (see main text for details).Energies are zero-point energy corrected

Tautomer	Energy (kJ/mol)	Tautomer	Energy (kJ/mol)
T1 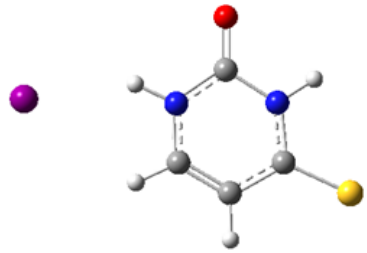	0.0	T4 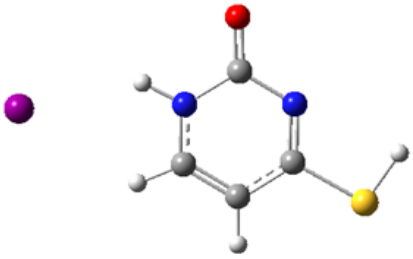	59.15
T2 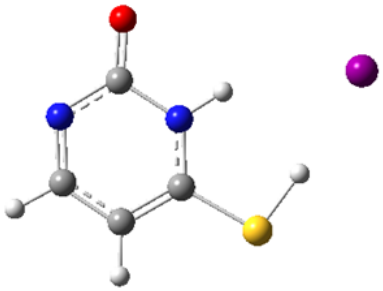	60.29	T5 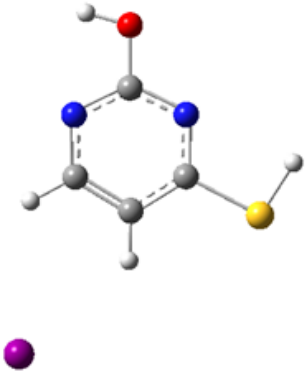	102.23
T3 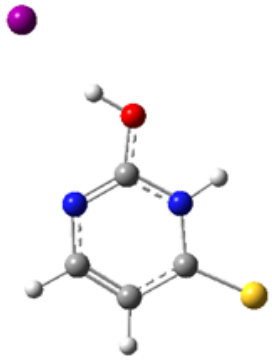	50.69	T6 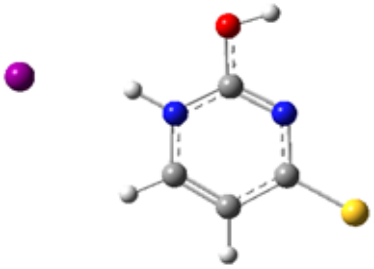	69.20

References

1. A. Les and L.Adamowicz, J. Am. Chem. Soc. , **112**, 1504-1509 (1990).

S2: Direction of the dipole moment of the TU molecule in the I^-·TU clusters

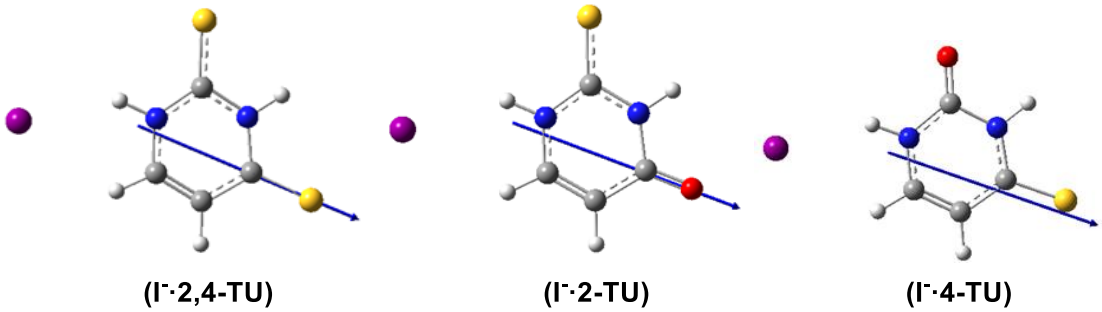

Fig. S1 The vector direction of the axis of the dipole moment of the TU molecule, calculated for the neutral uncomplexed molecule at the geometry of the optimized ion-molecule complex.

S3: Solution-phase absorption spectra of the I^-·TU clusters

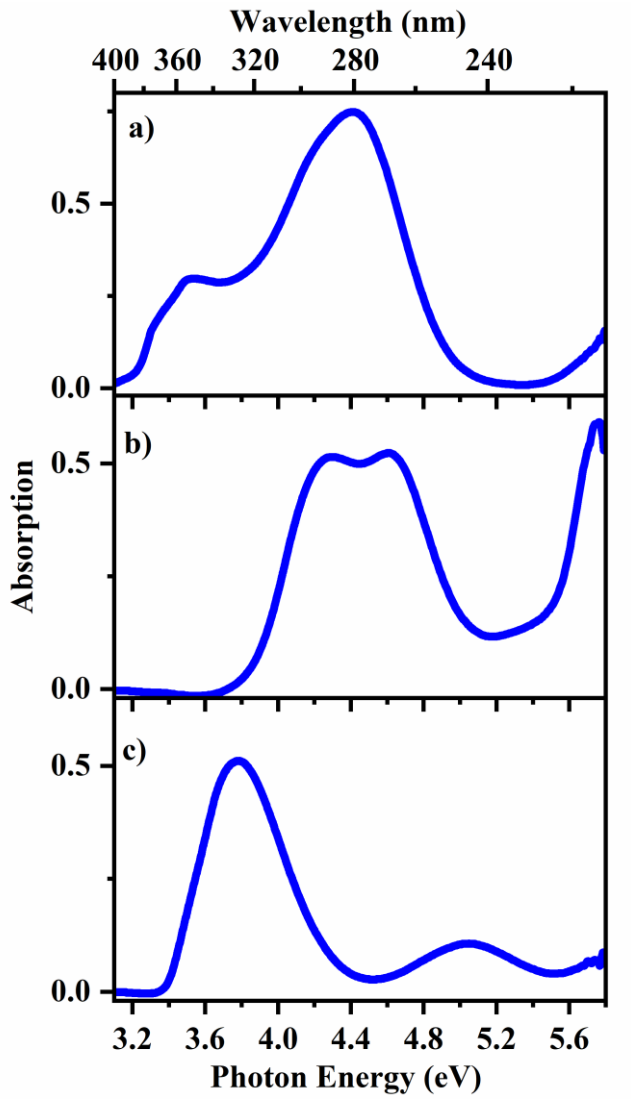

Fig. S2 Aqueous absorption spectrum of (a) 2,4-TU, (b) 2-TU and (c) 4-TU across the range 3.1 – 5.8 eV (400 – 213 nm).

S4: Higher collisional dissociation of I^{-}·TU clusters

Higher energy collisional dissociation (HCD) was performed on isolated I^{-}·TU clusters to determine the ground state thermal fragments. Fig, S4 displays as a function of applied % HCD energy, the relative intensities of the I^{-}·TU clusters parent ion and fragments production intensities respectively.

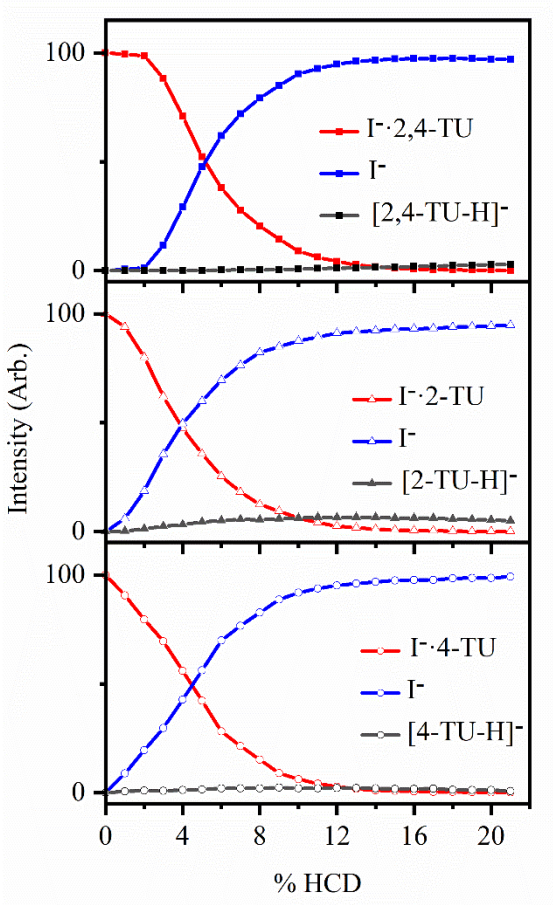

Fig. S4. Parent ion dissociation curve for I^{-}·2,4-TU, I^{-}·2-TU and I^{-}·4-TU alongside production curves of fragments upon HCD between 0 and 20% energy. The data points fitted with the curved lines are viewing guides to show the profile for an individual fragment.

S5: Electron detachment spectra of I^{-}·TU clusters

Electron detachment (ED) yield of I^{-}·TU clusters are displayed in Fig S5. Although electron loss cannot be directly measured in our instrument, we calculate it by assuming that any photodepleted ions that is not detected as an ionic-fragments are electron loss. (Note that our instrument can only detect ions with m/z >50.) Therefore, our calculated electron detachment yield is an upper limit on the true electron detachment yield, and should be treated as an estimated yield rather than an absolute measurement.

ED = (Photodepletion ion count -∑Photofragment ion count)

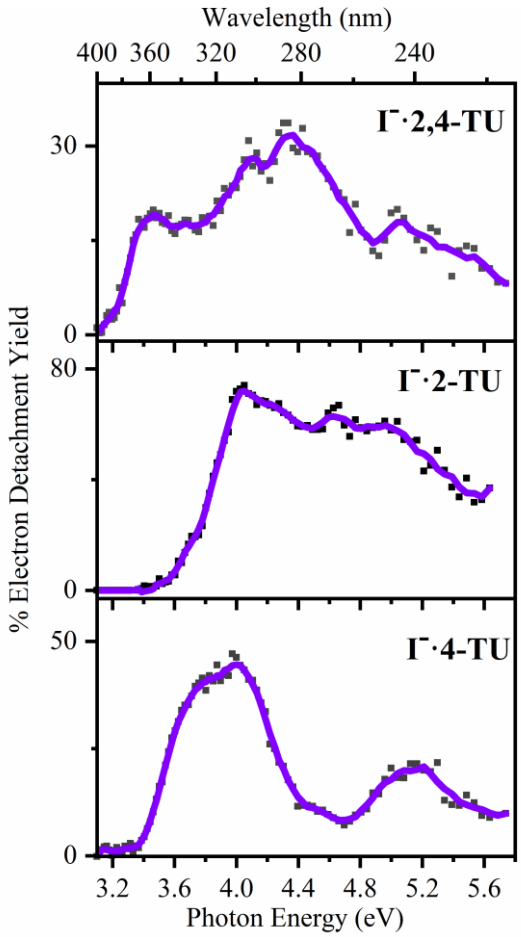

Fig. S5 % Electron Detachment yield of I^{-}·2,4-TU, I^{-}·2-TU and I^{-}·4-TU clusters. The solid line is a five-point adjacent average of data point.

S6: Time dependent density functional theory data of tautomers of the I^{-}·TU clusters

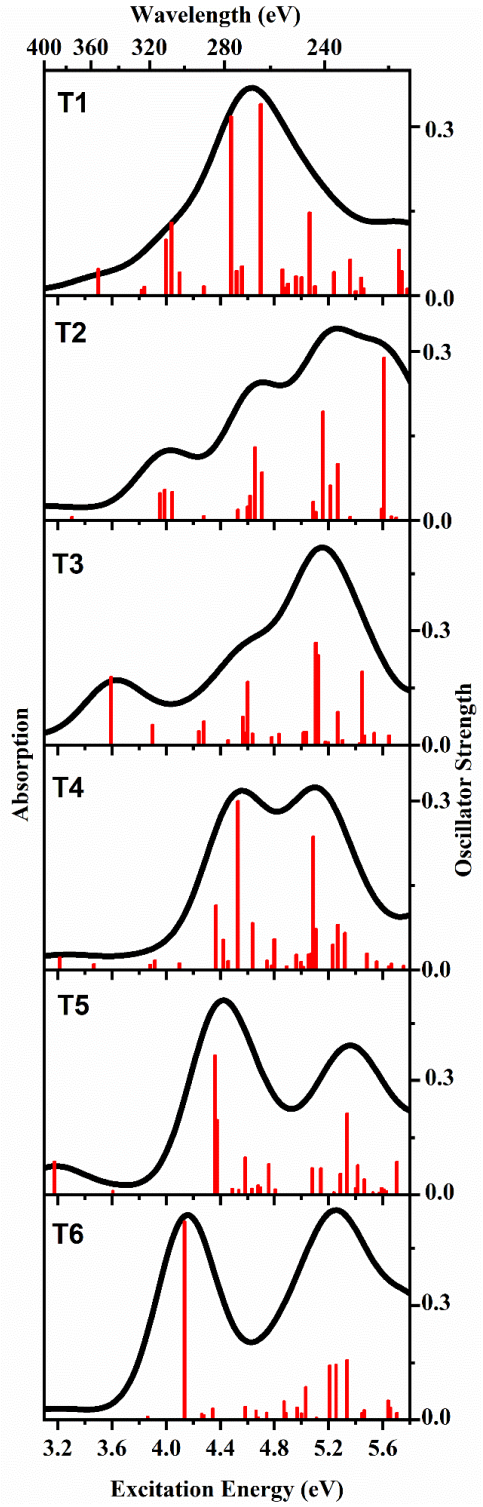

Fig. S6 TDDFT excitation spectra of the tautomers of I^{-}·2,4-TU clusters for the structures shown in Table S1. The oscillator strengths (OSC.) on the y axis of individual transitions ≥ 0.005 within the experimental scan range are shown by vertical bars while the full line spectrum is a convolution of the calculated spectrum with Gaussian function (0.25 eV HWHM).

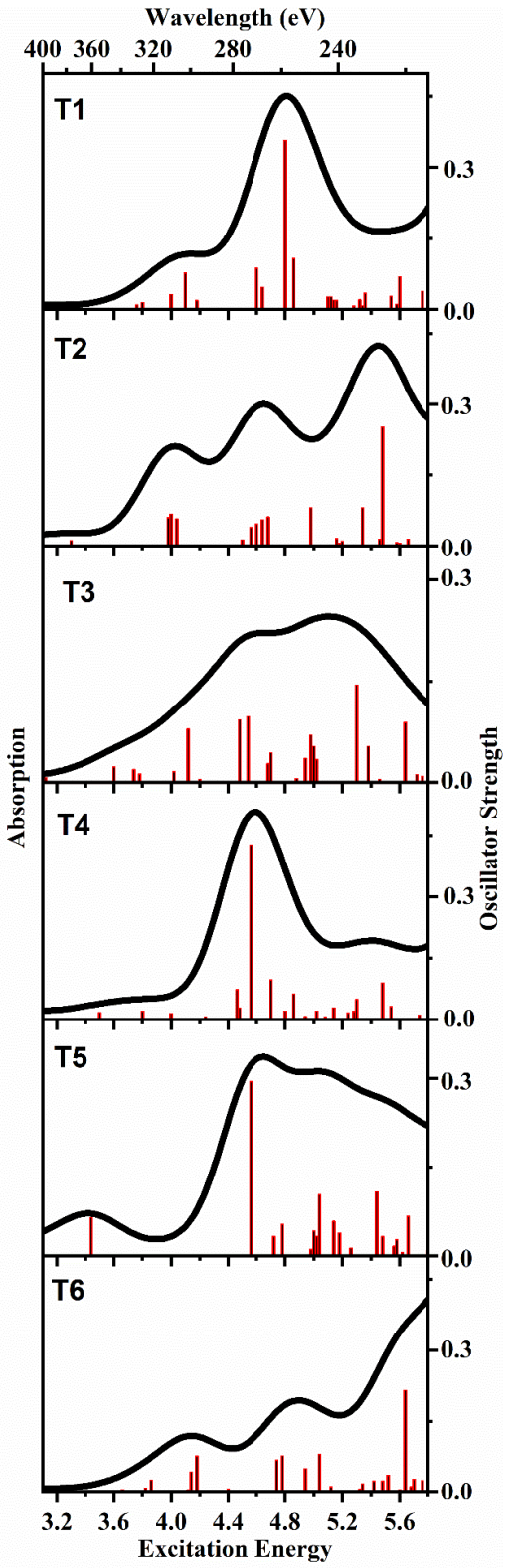

Fig. S7 TDDFT excitation spectra of the tautomers of I^{-}·2-TU clusters for the structures shown in Table S2. The oscillator strengths (OSC.) on the y axis of individual transitions ≥ 0.005 within the experimental scan range are shown by vertical bars while the full line spectrum is a convolution of the calculated spectrum with Gaussian function (0.25 eV HWHM).

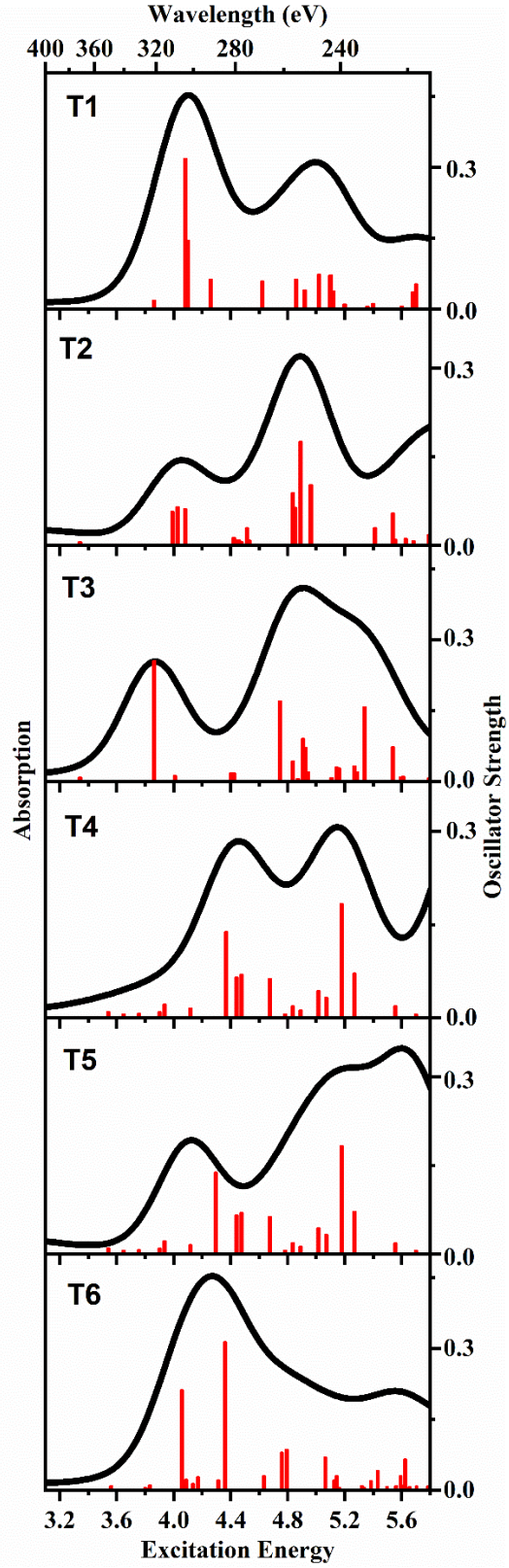

Fig. S8 TDDFT excitation spectra of the tautomers of I^{-}·4-TU clusters for the structures shown in table S2. The oscillator strengths (OSC.) on the y axis of individual transitions ≥ 0.005 within the experimental scan range are shown by vertical bars while the full line spectrum is a convolution of the calculated spectrum with Gaussian function (0.25 eV HWHM).

S7: Equation-of-motion coupled-cluster singles and doubles calculations of I^{-}·2-TU cluster

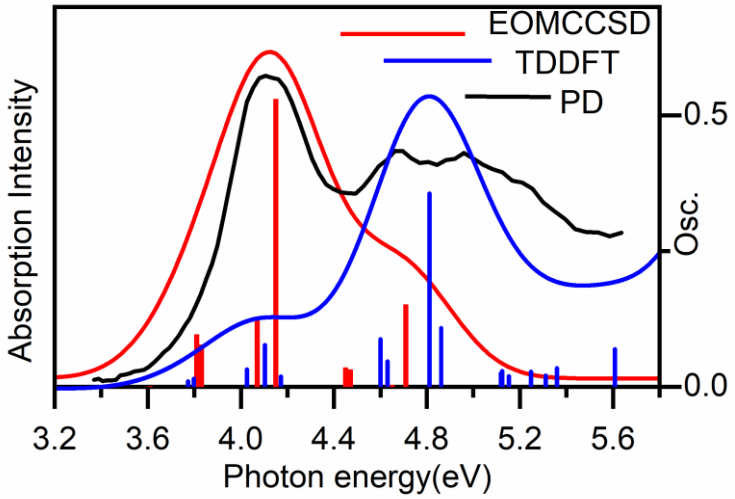

Fig. S9 Overlaid EOMCCSD, TDDFT and photodepletion spectrum of I^{-}·2-TU to explore the dipole-bound state.

S8: Molecular orbitals involved in the TDDFT transitions of I^{-}·TU clusters

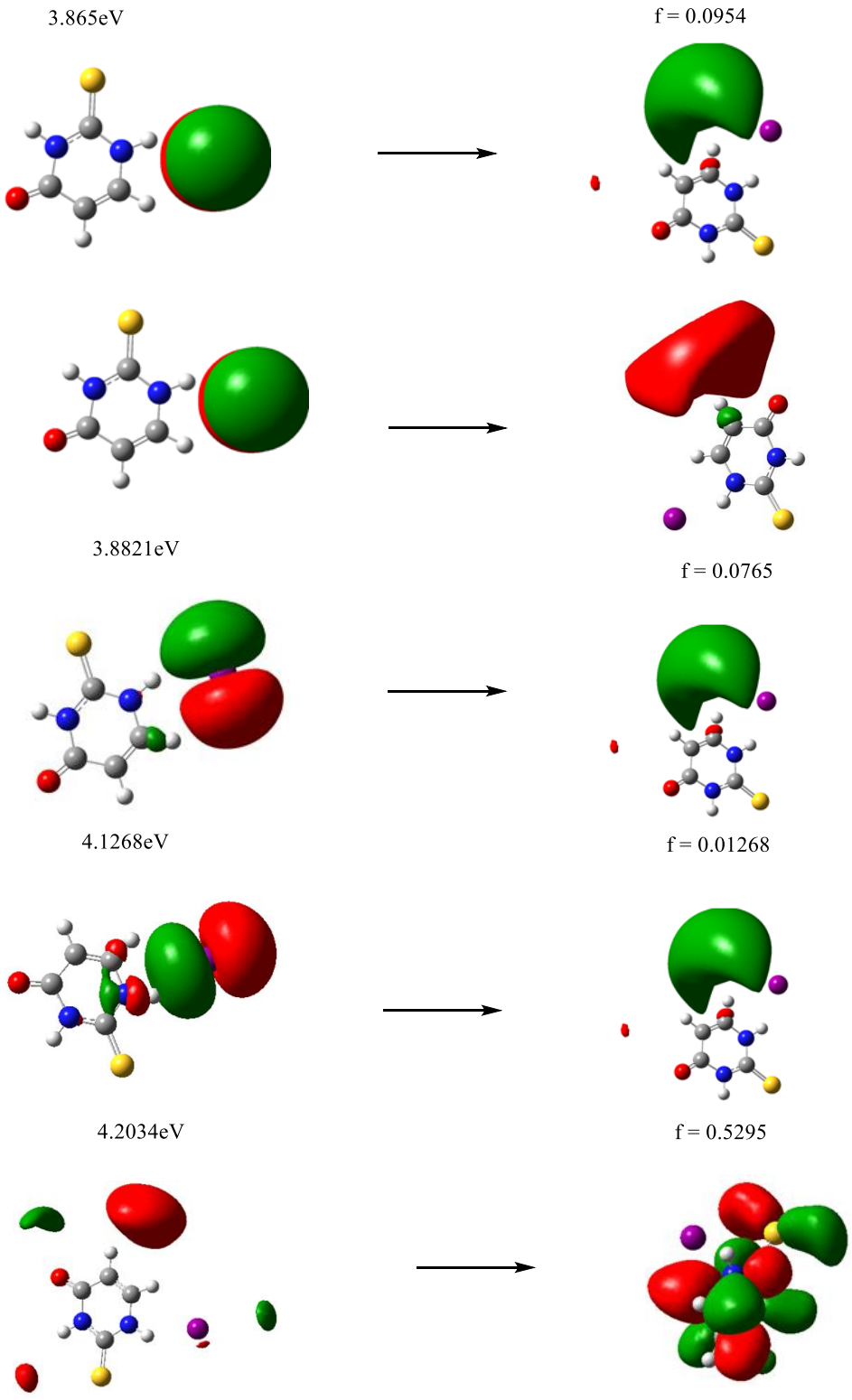

Fig. S10 Molecular orbital transitions I^{-}·2-TU involved in the dipole-bound excited state predicted by EOMCCSD calculations between 3.87 – 4.21 eV. The excitation energies are offset by – 1.12 eV for comparison with the experimental data.

Table S4 Calculated TDDFT transition energies at the B3LYP/6-311++G(2d,2p)/SDD level of theory and oscillator strengths of the I^{-}·2,4-TU cluster. Only transitions below 5.7 eV with oscillator strength > 0.005

Orbital transitions	ΔE (eV)	f
(0.26)35(π)→42(π*)	3.51	0.0470
(0.65)37(π)→42(π*)		
(0.69)41(n)→44(σ*)	3.81	0.0102
(0.69)40(n)→44(σ*)	3.84	0.0151
(0.53)35(π)→42(π*)	4.05	0.1301
(0.35)37(π)→43(π*)		
(0.26)35(π)→43(π*)		
(0.69)39(n)→44(σ*)	4.09	0.0407
(0.69)40(n)→45(π*)	4.29	0.0159
(0.34)35(π)→42(π*)	4.47	0.3131
(0.36)35(π)→43(π*)		
(0.35)37(π)→43(π*)		
(0.22)39(n)→45(π*)		
(0.20)37(π)→42(π*)		
(0.66)39(n)→45(π*)	4.52	0.0428
(0.63)41(n)→46(σ*)	4.57	0.0518
(0.25)41(n)→48(σ*)		
(0.46)35(π)→43(π*)	4.71	0.3399
(0.43)37(π)→43(π*)		
(0.22)40(n)→46(σ*)		
(0.63)39(n)→46(σ*)	4.85	0.0462
(0.24)39(n)→48(σ*)		
(0.66)41(n)→47(σ*)	4.87	0.0134
(0.67)40(n)→47(σ*)	4.90	0.0207
(0.60)41(n)→48(σ*)	4.96	0.0339
(0.24)41(n)→46(σ*)		
(0.21)41(n)→47(σ*)		

(0.61)40(n)→48(σ*)	4.99	0.0321
(0.23)40(n)→46(σ*)		
(0.65)38(n_s)→44(σ*)	5.07	0.1476
(0.67)40(n)→50(σ*)	5.16	0.0159
(0.61)39(n)→48(σ*)	5.24	0.0413
(0.23)39(n)→47(σ*)		
(0.22)39(n)→46(σ*)		
(0.63)36(π)→44(σ*)	5.35	0.0636
(0.21)38(n_s)→45(π*)		
(0.64)41(n)→51(σ*)	5.41	0.0075
(0.65)35(π)→44(σ*)	5.45	0.0313
(0.60)40(n)→51(σ*)	5.46	0.0123
(0.21)40(n)→53(σ*)		
(0.61)41(n)→52(σ*)	5.61	0.0068

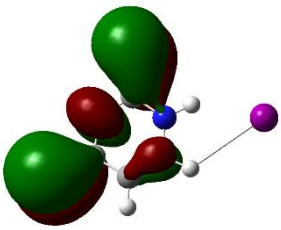

MO 35

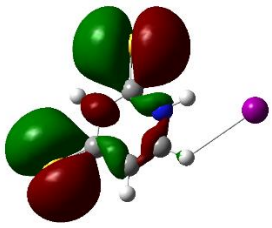

MO 36

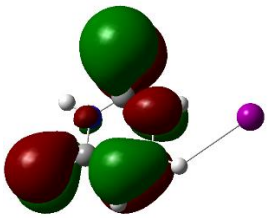

MO 37

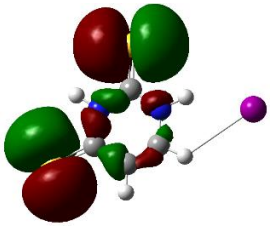

MO 38

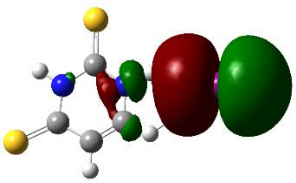

MO 39

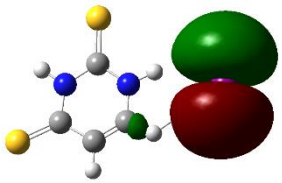

MO 40

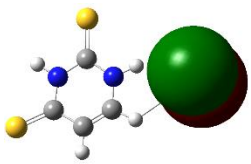

MO 41

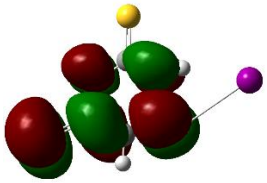

MO 42

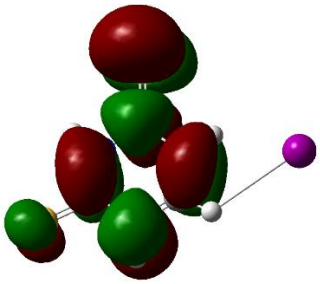

MO 43

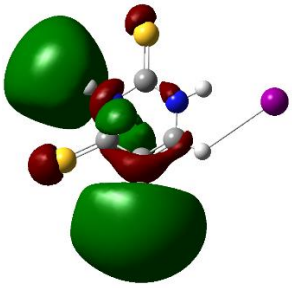

MO 44

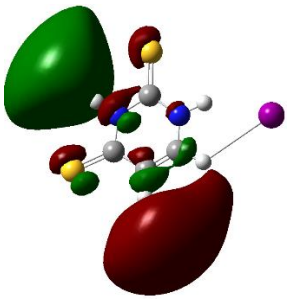

MO 45

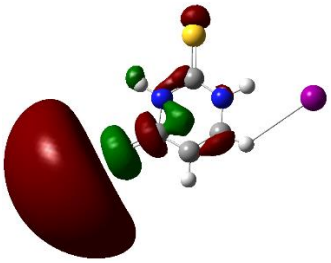

MO 46

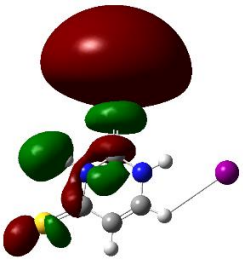

MO 47

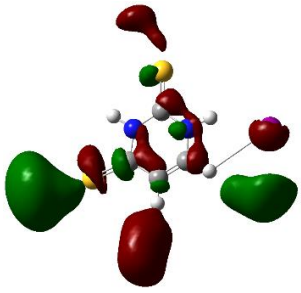

MO 48

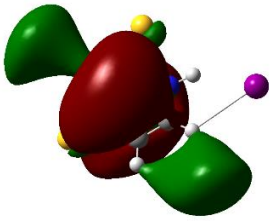

MO 50

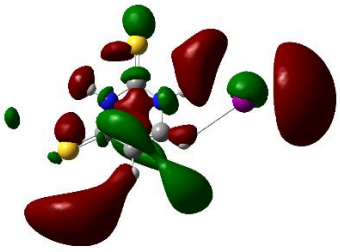

MO 51

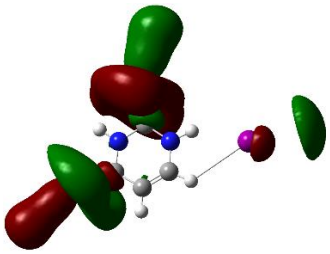

MO 53

Table S5 Calculated TDDFT transition energies at the B3LYP/6-311++G(2d,2p)/SDD level of theory and oscillator strengths of the I^{-}·2,4-TU cluster. Only transitions below 5.6 eV with oscillator strength > 0.005

Orbital transitions	ΔE (eV)	f
(0.26)35(π)→42(π*)	3.51	0.0470
(0.65)37(π)→42(π*)		
(0.69)41(n)→44(σ*)	3.81	0.0102
(0.69)40(n)→44(σ*)	3.84	0.0151
(0.53)35(π)→42(π*)	4.05	0.1301
(0.35)37(π)→43(π*)		
(0.26)35(π)→43(π*)		
(0.69)39(n)→44(σ*)	4.09	0.0407
(0.69)40(n)→45(π*)	4.29	0.0159
(0.34)35(π)→42(π*)	4.47	0.3131
(0.36)35(π)→43(π*)		
(0.35)37(π)→43(π*)		
(0.22)39(n)→45(π*)		
(0.20)37(π)→42(π*)		
(0.66)39(n)→45(π*)	4.52	0.0428
(0.63)41(n)→46(σ*)	4.57	0.0518
(0.25)41(n)→48(σ*)		
(0.46)35(π)→43(π*)	4.71	0.3399
(0.43)37(π)→43(π*)		
(0.22)40(n)→46(σ*)		
(0.63)39(n)→46(σ*)	4.85	0.0462
(0.24)39(n)→48(σ*)		
(0.66)41(n)→47(σ*)	4.87	0.0134
(0.67)40(n)→47(σ*)	4.90	0.0207
(0.60)41(n)→48(σ*)	4.96	0.0339
(0.24)41(n)→46(σ*)		
(0.21)41(n)→47(σ*)		

(0.61)40(n)→48(σ*)	4.99	0.0321
(0.23)40(n)→46(σ*)		
(0.65)38(n_s)→44(σ*)	5.07	0.1476
(0.67)40(n)→50(σ*)	5.16	0.0159
(0.61)39(n)→48(σ*)	5.24	0.0413
(0.23)39(n)→47(σ*)		
(0.22)39(n)→46(σ*)		
(0.63)36(π)→44(σ*)	5.35	0.0636
(0.21)38(n_s)→45(π*)		
(0.64)41(n)→51(σ*)	5.41	0.0075
(0.65)35(π)→44(σ*)	5.45	0.0313
(0.60)40(n)→51(σ*)	5.46	0.0123
(0.21)40(n)→53(σ*)		
(0.61)41(n)→52(σ*)	5.61	0.0068

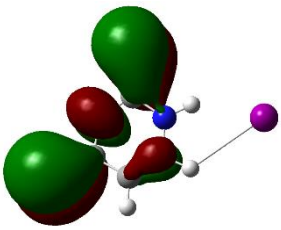

MO 35

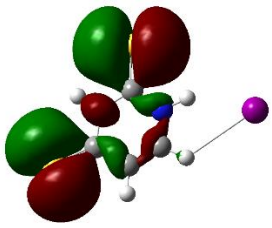

MO 36

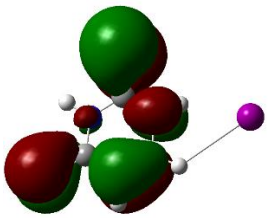

MO 37

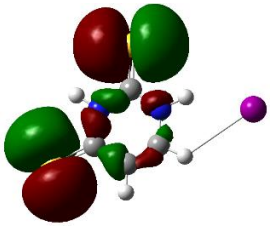

MO 38

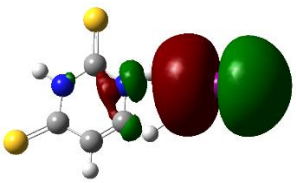

MO 39

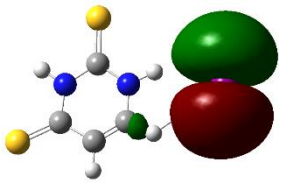

MO 40

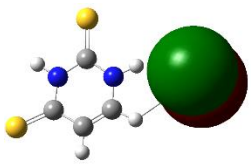

MO 41

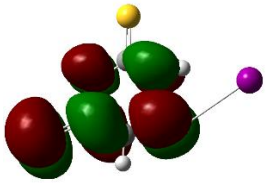

MO 42

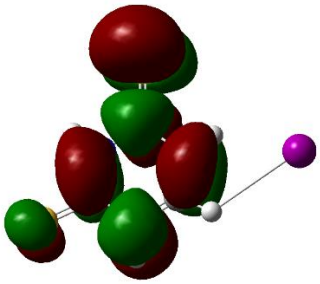

MO 43

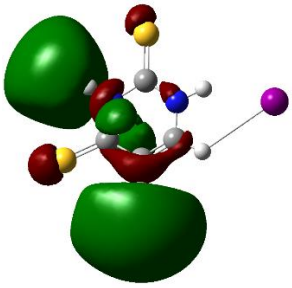

MO 44

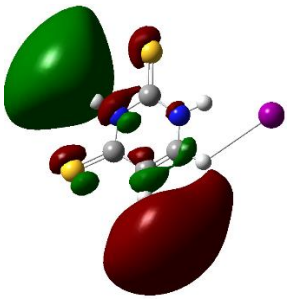

MO 45

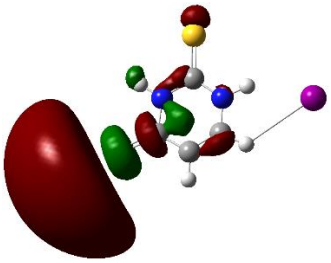

MO 46

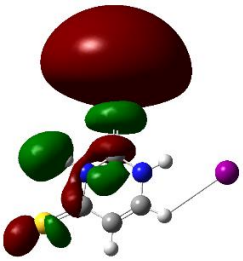

MO 47

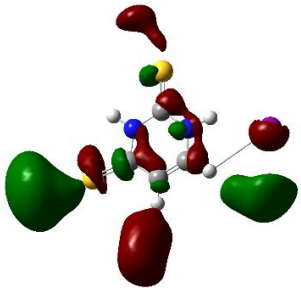

MO 48

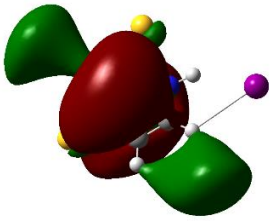

MO 50

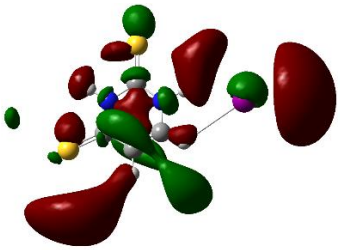

MO 51

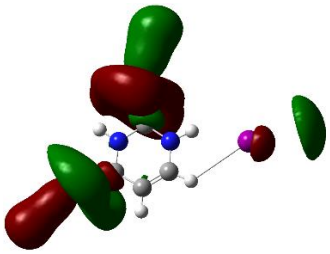

MO 53

Table S6 Calculated TDDFT transition energies at the B3LYP/6-311++G(2d,2p)/SDD level of theory and oscillator strengths of the I^{-}·4-TU cluster. Only transitions below 5.7 eV with oscillator strength > 0.005

Orbital transitions	ΔE (eV)	f
(0.71)37(n)→39(π*)	3.66	0.0067
(0.69)37(n)→40(σ*)	3.82	0.0091
(0.69)36(n)→40(σ*)	3.85	0.0177
(0.52)35(n)→40(σ*)	4.09	0.3181
(0.44)33(π)→38(π*)		
(0.52)33(π)→38(π*)	4.11	0.1450
(0.46)35(n)→40(σ*)		
(0.69)37(n)→41(π*)	4.22	0.0059
(0.69)36(n)→42(σ*)	4.26	0.0173
(0.62)37(n)→42(σ*)	4.58	0.0618
(0.31)37(n)→43(σ*)		
(0.62)36(π)→42(σ*)	4.62	0.0583
(0.31)36(π)→43(σ*)		
(0.62)35(n)→42(σ*)	4.86	0.0626
(0.31)35(n)→43(σ*)		
(0.61)37(n)→43(σ*)	4.92	0.0395
(0.33)37(n)→42(σ*)		
(0.61)36(n)→43(σ*)	4.95	0.0309
(0.33)36(n)→42(σ*)		
(0.68)34(n_s)→40(σ*)	5.03	0.0727
(0.60)33(π)→39(π*)	5.11	0.0716
(0.24)36(n)→45(σ*)		
(0.20)37(n)→44(π*)		
(0.43)36(n)→45(σ*)	5.12	0.0376
(0.43)37(n)→44(π*)		
(0.31)33(π)→39(π*)		
(0.47)37(n)→44(π*)	5.16	0.0200

(0.45)36(n)→45(σ*)		
(0.58)35(n)→43(σ*)	5.19	0.0097
(0.30)35(n)→42(σ*)		
(0.67)35(n)→45(σ*)	5.36	0.0051
(0.53)37(n)→47(σ*)	5.40	0.0112
(0.37)37(n)→46(σ*)		
(0.58)36(n)→47(σ*)	5.45	0.0079
(0.29)36(n)→46(σ*)		
(0.70)33(n)→41(π*)	5.61	0.0054
(0.63)34(n_s)→42(σ*)	5.68	0.0354
(0.67)34(n_s)→43(σ*)		
(0.45)35(n)→47(σ*)	5.69	0.0526
(0.43)35(n)→46(σ*)		

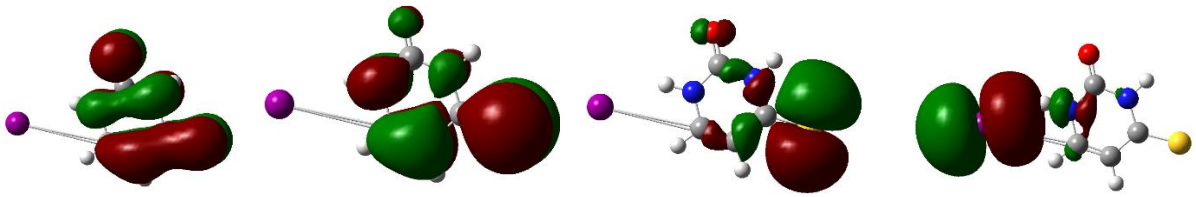

MO 32 MO 33 MO 34 MO 35

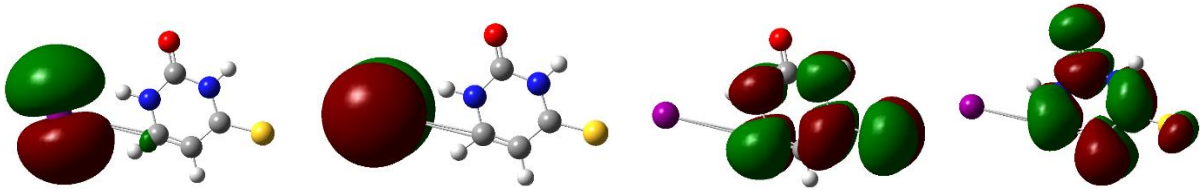

MO 36 MO 37 MO 38 MO 39

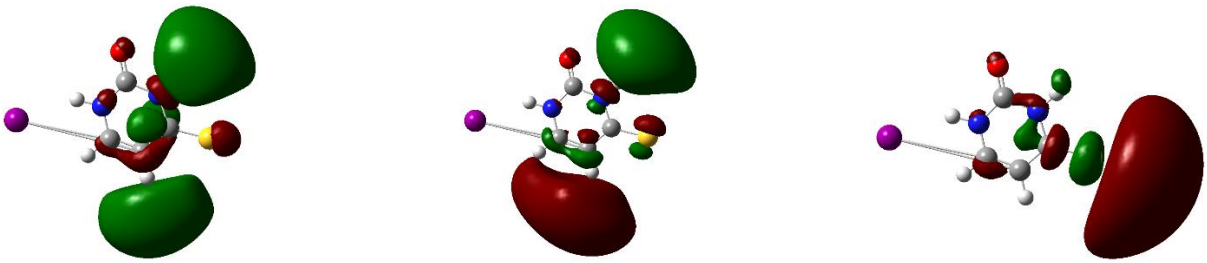

MO 40

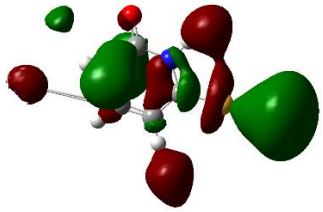

MO 41

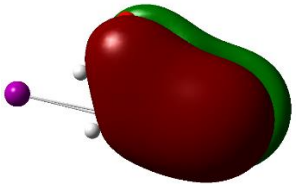

MO 42

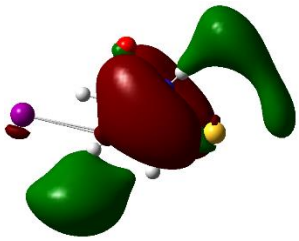

MO 43

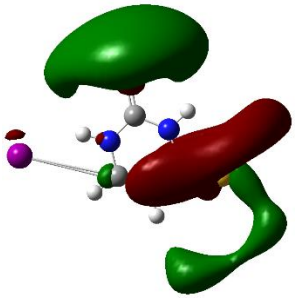

MO 44

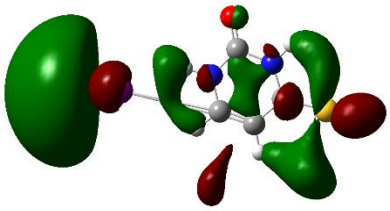

MO 45

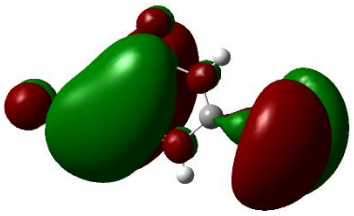

MO 46

MO 47

MO 48

Note: The $\mathbf{n_s}$ are transitions from non-bonding orbital of the sulphur atom while **n** is the iodide n ($5p^6$)